1   **The role of glutathione in periplasmic redox homeostasis and oxidative protein folding**

2   **in *Escherichia coli***

3

4   Lisa R. Knoke[1], Jannik Zimmermann[2], Natalie Lupilov[1] Jannis F. Schneider[1], Beyzanur

5   Celebi[1], Bruce Morgan[2] and Lars I. Leichert[1]

6   [1] Ruhr University Bochum, Institute of Biochemistry and Pathobiochemistry, Microbial

7   Biochemistry, Bochum, Germany

8   [2] Institute of Biochemistry, Centre for Human and Molecular Biology (ZHMB), Saarland

9   University, 66123 Saarbrücken, Germany

10

11   *Corresponding author: Lars I. Leichert; lars.leichert@ruhr-uni-bochum.de

Abstract

The thiol redox balance in the periplasm of *E. coli* depends on the DsbA/B pair for oxidative power and the DsbC/D system as its complement for isomerization of non-native disulfides. While the standard redox potentials of those systems are known, the *in vivo* redox potential imposed onto protein thiol disulfide pairs in the periplasm remains unknown. Here, we used genetically encoded redox probes (roGFP2 and roGFP-iL), targeted to the periplasm, to directly probe the thiol redox homeostasis in this compartment. These probes contain two cysteine residues, that are virtually completely reduced in the cytoplasm, but once exported into the periplasm, can form a disulfide bond, a process that can be monitored by fluorescence spectroscopy. Even in the absence of DsbA, roGFP2, exported to the periplasm, was fully oxidized, suggesting the presence of an alternative system for the introduction of disulfide bonds into exported proteins. However, the absence of DsbA shifted the periplasmic thiol-redox potential from -228 mV to a more reducing -243 mV and the capacity to re-oxidize periplasmic roGFP2 after a reductive pulse was significantly decreased. Re-oxidation in a DsbA strain could be fully restored by exogenous oxidized glutathione (GSSG), while reduced GSH accelerated re-oxidation of roGFP2 in the WT. In line, a strain devoid of endogenous glutathione showed a more reducing periplasm, and was significantly worse in oxidatively folding PhoA, a native periplasmic protein and substrate of the oxidative folding machinery. PhoA oxidative folding could be enhanced by the addition of exogenous GSSG in the WT and fully restored in a Δ*dsbA* mutant. Taken together this suggests the presence of an auxiliary, glutathione-dependent thiol-oxidation system in the bacterial periplasm.

Introduction

Extracellular proteins are stabilized by structural disulfide bonds that are introduced during oxidative protein folding. Thus, the correct folding of most of the proteins translocated into the periplasm and beyond in the model bacterium *Escherichia coli* depends on the formation of native disulfide bonds. The major pathway for introducing disulfide bonds in the periplasm of *E. coli* involves the DsbA-DsbB thiol oxidase system (Bardwell et al., 1993, 1991; Collet and Bardwell, 2002; Missiakas et al., 1993; Wunderlich and Glockshuber, 1993). DsbA contains a thioredoxin-like domain including an active site CxxC motif with a standard redox potential of around –122 mV (Martin et al., 1993; Wunderlich et al., 1993). After disulfide introduction, DsbA itself is re-oxidized by the integral membrane protein DsbB, which in turn is connected to the ubiquinone pool of the bacterial plasma membrane (Christensen et al., 2016; Inaba et al., 2009; Inaba and Ito, 2008; Manta et al., 2019; Vivian et al., 2009). As some proteins contain multiple cysteine residues, cells require quality control systems to isomerize non-native disulfide bonds. In *E. coli*, this system includes the disulfide isomerase DsbC/G and the reductive power from DsbD, which itself is coupled to the cytoplasmic NADPH pool through Thioredoxin A (TrxA) (Andersen et al., 1997; Cho and Collet, 2013; Missiakas et al., 1994; Rietsch et al., 1997; Shevchik et al., 1994; Sone et al., 1997).

In eukaryotes, oxidative folding in the endoplasmic reticulum (ER) is catalyzed in a similar manner by protein disulfide isomerase(s) (PDI), which also contains thioredoxin-like domains. Unlike DsbA, PDI not only acts as thiol oxidase but also functions as a disulfide reductase/isomerase (Ali Khan and Mutus, 2014; Ushioda and Nagata, 2019). PDI is re-oxidized for example by the sulfhydryl oxidase Endoplasmic reticulum oxidoreductin 1 (ERO1-Lα) (Tu and Weissman, 2004).

The tripeptide glutathione (GSH) is the most abundant low molecular weight thiol in many domains of life ranging from bacteria to eukaryotes (Fahey et al., 1978; Smirnova and

58   Oktyabrsky, 2005; Zechmann et al., 2011) and usually it is noted for its reductive properties,

59   keeping the cytoplasm reduced. In its reducing role, glutathione is oxidized to glutathione

60   disulfide (GSSG) (Aslund et al., 1994; Carmel-Harel and Storz, 2000; Masip et al., 2006). In

61   *E. coli*, cytosolic GSH levels have been described to be in the millimolar range (up to

62   10 mM). The GSH:GSSG ratio ranges from 50:1 to 200:1 and is maintained by the

63   glutathione reductase Gor, dependent on the cellular NADPH-pool (Åslund et al., 1999;

64   Fahey et al., 1978; Greer and Perham, 1986; Masip et al., 2006; Meister, 1988; Tuggle and

65   Fuchs, 1985).

66   Exponentially growing *E. coli* cells extensively secrete GSH into the culture medium. Several

67   ABC-transporters mediate GSH transport across the inner cell membrane and outer membrane

68   porins, allow GSH or GSSG to enter or leave the periplasm with around 10 % of all

69   synthesized GSH being secreted. (Holyoake et al., 2016; Pittman et al., 2005; Smirnova et al.,

70   2012; Suzuki et al., 2005; Wang et al., 2018). Although glutathione synthesis is restricted to

71   the cytosol, it is exported into the periplasm of *E. coli* and periplasmic glutathione probably

72   accounts for 10–30% of total cellular GSH (Eser et al., 2009; Pittman et al., 2005; Smirnova

73   et al., 2012). It has been suggested that the GSH:GSSG ratio in the periplasm reflects the

74   GSH:GSSG ratio of the culture medium, being approximately 16:1 (Eser et al., 2009; Pittman

75   et al., 2005; Smirnova et al., 2012, 2020, 2005; Song et al., 2021).

76   Since redox processes in the cell are highly regulated, the presence of glutathione in the

77   periplasm at such high levels strongly indicates that this molecule also plays a role in the

78   redox homeostasis of the periplasm, similar to its role in the ER (Birk et al., 2013; Delaunay-

79   Moisan et al., 2017). In fact, impaired GSH synthesis or reduced GSH import into the

80   periplasm is connected to several phenotypes, similar to those found in cells lacking the

81   DsbA/DsbB- or DsbC-system (Fabianek et al., 2000; Pittman et al., 2005). However, a direct

82   involvement in disulfide bond formation and redox homeostasis for GSH in the periplasm has

83   not yet been established.

84   Here, we explore the role of GSH in oxidative protein folding and redox homeostasis in the

85   periplasm of *E. coli* by targeting genetically encoded redox-sensitive probes with an

86   engineered disulfide bond to this compartment and analyzing the periplasmic redox dynamics

87   in the presence or absence of DsbA and/or GSH. We provide evidence that GSH indeed plays

88   a key role in disulfide bond formation and redox homeostasis in the periplasm: We observed

89   that GSSG can complement for the loss of DsbA and, unexpectedly, that GSH accelerates

90   disulfide bond formation in the presence of DsbA. In line, the periplasmic redox balance of

91   GSH-deficient cells was slightly shifted to a more reducing redox potential and the oxidative

92   folding of native DsbA substrates in these cells is impaired.

93 **Materials and methods:**

94 *Strains, Plasmids and growth conditions*

95 Bacterial strains and plasmids used in this study are listed in Supplementary tables S1 and S2.

96 *Escherichia coli* DH5α served as host for plasmid construction and storage and *E. coli* BL21

97 (DE3) was used for DsbA and *E. coli* MG1655 for roGFP2 recombinant protein production.

98 All *E. coli* strains used in this study were routinely cultivated at 37 °C in Luria-Bertani (LB)

99 medium, supplemented with antibiotics when required for plasmid maintenance and marker

100 selection (ampicillin 200 µg/mL or kanamycin 100 µg/mL), if not stated differently.

101 Protein expression in BL21 was induced with 0.4 mM IPTG when the cultures reached an

102 OD_{600} of ∼0.6–0.8 at 37 °C in LB medium and then incubated for 20 h at 20 °C after

103 induction.

104 *E. coli* mutants from the KEIO collection were used for construction of double deletion strains

105 and analysis of the periplasmic redox state (Baba et al., 2006). For expression of the redox

106 probes, mutant strains (Suppl. Table 1) harboring roGFP-based sensor protein-coding

107 plasmids (pPT_*roGFP2* or pPT_*roGFP-iL*, Supplementary table S2) were cultivated in

108 MOPS minimal medium (Technova, Hollister, CA, USA) at 37 °C until an optical density

109 (OD) of ∼0.5–0.8 was reached. Sensor protein expression was induced with 0.2 mM IPTG

110 and cells were cultivated for 16 h at 20 °C.

111 *Construction of different roGFP and DsbA expression vectors*

112 For construction of the pPT plasmid enabling periplasmic targeting, the *torA* sequence was

113 PCR amplified using appropriate primers (Supplementary table S3) from genomic *E. coli*

114 DNA (strain MC4100) and cloned into the pCC plasmid (Nilewski et al., 2021) using the

115 introduced *Nde*I 3' and 5' restriction sites. The *Nde*I restriction site upstream of *torA* was then

116 removed by QuickChange mutagenesis (Agilent, Waldbronn, Germany) according to the

117 manufacturer's protocol using primers QC-*Nde*I-fw and QC-*Nde*I-rv (Supplementary table

118 S3) resulting in the pPT plasmid.

119 In order to target roGFP2 into the periplasm, *roGFP2* was PCR amplified using the primer

120 pair listed in supplementary table S3 from the pCC_*roGFP2* plasmid as template. The

121 introduced *Nde*I and *Eco*RI restriction sites were used to clone the gene into the pPT-plasmid

122 resulting in pPT_*roGFP2* coding for a TorA_roGFP2 fusion protein.

123 The *roGFP-iL* gene was purchased from Addgene (Watertown, MA, USA) in a pQE30

124 plasmid harboring an ampicillin resistance gene. The *roGFP-iL* gene was PCR amplified

125 (Primers are listed in Supplementary table S3) with simultaneous introduction of *Xho*I and

126 *Eco*RI restriction sites. The amplified gene was cloned into the pPT plasmid using the

127 introduced restriction sites resulting in the plasmid pPT_*roGFP-iL* (pLK9).

128 For expression of a roGFP2-*Ec*DsbA(ΔSP) fusion protein, a truncated variant of the *dsbA*

129 (Δ*nt1-48*) gene was PCR amplified lacking the periplasmic sequence (ΔSP). The PCR

130 fragment was cut with *Eco*RI and *Hind*III. AtPrxA-ΔCP was removed from the

131 p416TEF_roGFP2-AtPrxA-ΔCP (Zimmermann et al., 2021) plasmid by the same restriction

132 enzymes and *Ec*DsbA(ΔSP) was cloned into the plasmid backbone, resulting in the plasmid

133 pLK16.

134 *Construction of E. coli dsbA, gshA double deletion strain by P1 transduction*

135 For the construction of an *E. coli gshA*, *dsbA* double mutant, the kanamycin cassette was

136 removed from the *gshA* KEIO mutant using the plasmid 709-FLPE as indicated by the

137 supplier (Gene Bridges, Heidelberg, Germany). Removal of the kanamycin cassette was

138 verified by colony PCR using *k1, k2* and *gshA* primers listed in supplementary table S3. The

139 *dsbA* mutant from the KEIO collection (strain: JW3832) was used as P1 donor. P1

140 transduction was carried out as previously described (Thomason et al., 2007). Correct

7

141   insertion of *dsbA* deletion in marker free *ΔgshA* was checked using appropriate primers

142   (Supplementary table S3).

143   *Periplasmic roGFP2-based measurements in E. coli*

144   For determining the roGFP2 redox state in different *E. coli* WT, Δ*dsbA*, Δ*gshA* or

145   Δ*dsbA*Δ*gshA*, the cells were transformed with the pPT_roGFP2 plasmid encoding the

146   TorA(SP)-roGFP2 fusion construct. Correct periplasmic probe localization was verified by

147   fluorescence microscopy (Supplementary figure 1). After expression of roGFP2 for 16 h at

148   20 °C, as aforementioned, cells were harvested, washed in HEPES buffer (40 mM, pH 7.4)

149   and adjusted to an OD_{600} of 1.0 in HEPES buffer containing either 1 mM Aldrithriol-2

150   (Sigma-Aldrich, Darmstadt, Germany, CAS-2127-03-9, AT-2) (oxidation control), 10 mM

151   Dithiothreitol (Sigma-Aldrich, Darmstadt, Germany, CAS-3483-12-3, DTT) (reduction

152   control), or buffer. As AT-2 was solved in DMSO, the solvent was added to all samples.

153   100 µL of the *E. coli* suspensions were added to the wells of a black, clear-bottom 96-well

154   plate (Nunc, Rochester, NY). Fluorescence intensities were recorded using the Synergy H1

155   multi-detection microplate reader (Biotek, Bad Friedrichshall, Germany) at excitation

156   wavelengths 405 and 488 nm and emission wavelength at 525 nm at 25 °C. The ratios of the

157   fluorescence excitation intensities (405/488 nm) were used to calculate the probe's oxidation

158   state. All values were normalized to fully oxidized (AT-2-treated) and fully reduced (DTT-

159   treated) roGFP2 with the following equation [1]:

$$OxD = \frac{R - R_{red}}{\left(\dfrac{I_{488}ox}{I_{488}red}\right) * (R_{ox} - R) + (R - R_{red})}$$

160   with R_{ox} being the 405/488 ratio of oxidized (AT2-treated) and R_{red} of reduced (DTT-treated)

161   roGFP2 respectively. $I_{488}ox$ and $I_{488}red$ are the fluorescence intensities of roGFP2 at 488 nm

162   under oxidizing or reducing conditions. R is the measured 405/488 nm ratio of roGFP2 in the

163   respective bacterial strain under the respective condition.

8

164   For determining the re-oxidation capacity of roGFP2 in the periplasm of different *E. coli*

165   mutants after a reductive pulse, cells expressing roGFP2 were harvested, washed in HEPES

166   buffer and adjusted to an OD_{600} of 1.0 in HEPES buffer. Afterwards aliquots of the cell

167   suspension were treated with 10 mM DTT for 10 min at 25°C and the reductant was washed

168   out by three washing steps with HEPES buffer. The OD_{600} was again adjusted to 1.0 in

169   HEPES buffer. After transfer of 100 µL of the respective cell suspensions into a black, clear-

170   bottom 96-well plate (Nunc, Rochester, NY), 5 mM of the substances of interest: buffer,

171   reduced (Sigma-Aldrich, CAS-70-18-8, GSH) or oxidized (Sigma-Aldrich, CAS-27025-41-8,

172   GSSG) glutathione, cysteine or cystine, β-mercapthoethanol or DTT were added.

173   Fluorescence intensities were recorded as described above with 1 min 41 sec intervals for

174   180 min at 25 °C. Fully oxidized (AT-2-treated), fully reduced (DTT-treated) and untreated

175   cells, that were not pre-reduced were used to calibrate roGFP2. For calculation and

176   normalization of the probe's oxidation degree at each time point, the means of all values

177   recorded at all time points for R_{red}, R_{ox}, $I_{488}ox$ and $I_{488}red$ were used. Data was processed

178   using Microsoft Excel software and GraphPad Prism.

179   *Determination of the redox potential of roGFP-iL in the periplasm of E. coli*

180   The redox potential of roGFP-iL targeted to the periplasm of *E. coli* WT, *ΔdsbA*, *ΔgshA* or

181   *ΔdsbAΔgshA* by expression from pPT-*roGFP-iL* plasmid was determined as described

182   previously for cytosolic roGFP2 (Degrossoli et al., 2018; Gutscher et al., 2008; Xie et al.,

183   2020) or Grx1-roGFP2-iL located in the endoplasmic reticulum (Ugalde et al., 2022). Correct

184   probe localization was verified by fluorescence microscopy (Supplementary figure 1). Firstly,

185   *roGFP-iL* was expressed as described above for 16 h at 20 °C, cells were harvested, washed

186   in HEPES buffer (40 mM, pH 7.4) and adjusted to an OD_{600} of 1.0 in HEPES buffer. The

187   fluorescence intensity was recorded with continuous stirring every 30 sec for at least 5 min at

188   37 °C in an FP-8500 spectrofluorometer (Jasco, Tokyo, Japan) with a fixed emission

189   wavelength at 510 nm. The scanned excitation wavelength ranged from 350 to 500 nm.

190   Bandwidths of both, excitation and emission were set to 5 nm. The fluorescence excitation

191   ratios (395/465 nm) were used as measurement of probe oxidation (Lohman and Remington,

192   2008). For normalization, 1 mM AT-2 and 10 mM DTT were added to the cells achieving full

193   oxidation or reduction of the probe. For calculation, equation [1] was modified. R_{ox} was

194   395/465 ratio of oxidized and R_{red} of reduced roGFP-iL. $I_{465}ox$ and $I_{465}red$ represent the

195   fluorescence intensities of roGFP2 at 465 nm under oxidizing or reducing conditions. R is

196   the measured 395/465 nm ratio of roGFP-iL in the respective bacterial strain under the

197   respective conditions. All values used for calculation of R_{ox}, R_{red}, $I_{465}ox$ and $I_{465}red$ are the

198   mean of at least four measured time points, respectively.

199   The redox potential of roGFP-iL in the periplasm was calculated as previously described

200   (Ugalde et al., 2022; Xie et al., 2020) using the Nernst equation [2]:

$$E_{roGFPiL} = E^0_{roGFPiL} - \frac{R * T}{n * F} * \ln \left(\frac{1 - OxD_{roGFPiL}}{OxD_{roGFPiL}}\right)$$

201   with $E^0_{roGFPiL}$=-229 mV (Lohman and Remington, 2008). R is the gas constant

202   (8.314 J.K^{-1}mol^{-1}), T (310.15 K $\cong$ 25 °C), n is the number of transferred electrons (2) and F is

203   Faraday's constant (96'485 C mol^{-1}). Data was processed using Microsoft Excel software and

204   GraphPad Prism.

205   *Fluorescence Microscopy*

206   *E. coli* WT, Δ*dsbA*, Δ*gshA* or Δ*dsbA*Δ*gshA* cells producing either roGFP2 or roGFP-iL from

207   pPT plasmids cultivated as described above were harvested, washed and resuspended to an

208   OD$_{600}$ of 1.0 in PBS buffer (1.5 mM KH$_2$PO$_4$, NaCl 150 mM, 2.7 mM Na$_2$HPO$_4$-7xH$_2$O, pH

209   7.4). Afterwards, 2 µL of the cell suspension were spotted on a 1.5 % Agarose pad covering a

210   microscopy slide. *E. coli* WT cells producing roGFP2 from the pCC-roGFP2 plasmid served

211   as cytoplasmic control. For fluorescence microscopy and image acquisition an Olympus

10

212   BX51 microscope equipped with CCD camera (Retiga 3, QImaging), and LED light source

213   (SOLA-365, Lumencor) driven by VisiView 3.× (Visitron systems) software was used. Image

214   acquiring was carried out using a Plan-APO 100×/1.4 NA oil objective with the following

215   filter set: BP 450–488 nm, FT 495 nm, and BP 512–542 nm. The Image J software (Schneider

216   et al., 2012) was used for image processing.

217   *Intracellular roGFP2-based measurements in yeast cells*

218   YPH499 Δ*glr1*Δ*grx1*Δ*grx2* cells were transformed with a p415TEF-*OPT1* plasmid encoding

219   the glutathione transporter, Opt1/Hgt1, and a p416TEF plasmid encoding the indicated

220   roGFP2 fusion construct. Cells transformed with empty plasmids served as controls for the

221   subtraction of fluorescence background. Cells were grown at 30°C in Hartwell's complete

222   (HC) medium with 2% glucose and lacking leucine and uracil (-Leu-Ura) to ensure retention

223   of both plasmids to an OD_{600} of ~3.0. Cells were harvested by centrifugation at 1000 x *g* for

224   3 min at room temperature and resuspended in 2 mL fresh HC -Ura-Leu medium containing

225   50 mM DTT to reduce all roGFP2 sensors before the start of the experiment. Cells were then

226   incubated for 4 min at room temperature, centrifuged at 1000 x *g* for 3 min, washed once with

227   2 mL fresh HC -Ura-Leu medium and finally resuspended in fresh HC -Ura-Leu medium to

228   an OD_{600} of 7.5. The cell suspension was subsequently transferred to a flat-bottomed 96-well

229   plate, with 200 µl per well. The 96-well plate was centrifuged at 30 x *g* for 5 min so that cells

230   formed an even, loose pellet at the bottom of each well.

231   To calibrate the probe, fully oxidized and fully reduced samples were generated by the

232   addition of 20 mM *N,N,N',N'*-Tetramethylazodicarboxamide (diamide, *Sigma Aldrich*) or

233   100 mM Dithiotreitol (DTT, *AppliChem*), respectively. Glutathione disulfide (GSSG, *Sigma*

234   *Aldrich*) was added to experimental samples at final concentrations ranging from 1.5 µM to

235   100 µM. Probe responses were followed for 500 s in a BMG Labtech CLARIOstar[Plus]

236   fluorescence plate reader. All experiments were performed at least three times with cells from

237   independent cultures. The degree of roGFP2 oxidation was calculated according to equation

238   [1] with the exception that values were recorded at 400 and 480 nm instead of 405 and

239   488 nm.

240   *Purification of DsbAΔSP and roGFP2 from E. coli BL21 and enzymatic assay*

241   For DsbA *in vitro* assays, DsbA was expressed as N-terminally truncated variant lacking the

242   periplasmic signal peptide and N-terminally fused to a Strep-Tag with a TEV-cleavage site in

243   *E. coli* BL21 cells. The protein was purified with Strep-affinity chromatography (for more

244   details see supplementary figure 2), the tag was removed by TEV-cleavage and the protein

245   was dialyzed into buffer W (100 mM Tris-HCl, 150 mM NaCl, 1 mM EDTA, pH 8.0).

246   roGFP2 was expressed from pCC_*roGFP2* in *E. coli* MG1655 and purified as previously

247   described (Müller et al., 2017). DsbAΔSP was oxidized with a 10-fold molar excess of AT-2

248   and roGFP2 was reduced with a 10-fold molar excess of DTT for 10 min at 20 °C and then

249   the oxidant or reductant were removed using Micro Bio-Spin™ P-30 gel columns (BioRad,

250   Feldkirchen, Germany, #7326223) or NAP™-5 columns (Cytiva, Freiburg, Germany,

251   #17085302) according to the supplier's protocol. For kinetic measurements, 0.2 µM roGFP2

252   were incubated with buffer alone, a 20-fold molar excess of oxidized DsbAΔSP, GSSG or

253   both in a 96-well plate (Nunc, Rochester, NY). Addition of 2 µM AT-2 or DTT served as

254   calibration marks for fully reduced or oxidized roGFP2 for the calculation of the OxD,

255   according to equation [1]. roGFP2 fluorescence was recorded for 18 h at 25 °C in a Synergy

256   H1 multi-detection microplate reader (Biotek, Bad Friedrichshall, Germany) at the excitation

257   wavelengths 405 and 488 nm and emission wavelength at 525 nm with the following settings:

258   20 nm bandwidth, gain 75 %, intervals: 1 min 41 sec, optics: bottom. Data processing was

259   carried out as described above for cellular roGFP2 assays.

260   *PhoA activity assay and verification of PhoA synthesis*

261   Activity of alkaline phosphatase PhoA was measured as described previously (Brickman and

262   Beckwith, 1975) with modifications. Briefly, mutant strains were cultivated in 5 mL MOPS

263   minimal medium with appropriate antibiotics at 37 °C without or with supplementation of 5

264   mM GSH or GSSG for around 18 h. Afterwards, *A. dest*, 5 mM GSH or GSSG were added

265   again and the cells were incubated for one more hour. After incubation and measurement of

266   the OD_{600}, 100 mM iodoacetamide (Sigma-Aldrich, CAS-144-48-9, IAM) was added to 1 mL

267   of the culture and cells were left on ice for 20 min. Cells were harvested (16,000 x g, 4 °C, 2

268   min) and washed two times with 1 mL washing buffer (50 mM NaCl, 10 mM NH_4Cl, 10 mM

269    $MgCl_2$, 40 mM MOPS, 10 mM IAM, pH 7.3). Cell pellets were resuspended in 100 µL lysis

270   buffer (10 mM EDTA, 2 mg/mL lysozyme, 20 mM Tris-HCl, 10 mM IAM, pH 8.0) and

271   incubated for 30 min on ice. Afterwards, cells were lysed by three freeze and thaw cycles in

272   liquid nitrogen and a 37 °C waterbath, followed by addition of 900 µL resuspension buffer

273   (10 mM $MgCl_2$, 10 mM $ZnCl_2$, 1 M Tris-HCl, pH 8.0) and warming the samples to 28 °C.

274   0.04 % *p*-nitrophenylphosphate (Sigma-Aldrich, CAS- 333338-18-4) were added and samples

275   were incubated until the solution turned visibly yellow, before the reaction was stopped by

276   adding 200 µL 1 M K_2HPO_4. The time point of reaction stop was noted. Lysates were then

277   incubated on ice for 10 min and centrifuged for 5 min at 16,000 x g. The absorption at 420 nm

278   and 550 nm of the supernatant was measured against a mixture of 100 µL lysis buffer, 900 µL

279   resuspension buffer, 100 µL 0.4 % pNPP solution and 200 µL stop solution in a

280   BioSpectrophotometer (Eppendorf, Hamburg, Germany). The PhoA activity was calculated

281   using equation [3]:

$$AU = 1000 * \frac{Abs_{420} - 1.75 * Abs_{550}}{Time\ [min] * OD_{600}} * Dilution\ factor$$

282   with AU being arbitrary units, Abs being the absorption at 420 nm and 550 nm and OD_{600}

283   being the culture optical density at 600 nm.

13

284   For analysis of PhoA accumulation, 1 mL of each aforementioned cultures were harvested

285   and the pellet was resuspended in standard 1x SDS-sample buffer adjusted to 100 µL for an

286   OD_{600} of 1.0. PhoA accumulation was analyzed by SDS-PAGE (NuPAGE™ 4 bis 12 %, Bis-

287   Tris, Invitrogen, Waltham, MA, USA) and Western blot analyses were carried out using

288   nitrocellulose membranes in the iBLOT2 system (Invitrogen, Waltham, MA, USA), both

289   according to the supplier. For detection on Western blot, a PhoA-specific first antibody

290   (Sigma-Aldrich, #MAB1012 1:5'000) and a goat-anti-mouse IRDye 800CW conjugate

291   (LeiCor, Lincoln, NE, USA, #926-32210) were used (1:5'000) according to the supplier's

292   protocol. Proteins were detected by fluorescence using the Sapphire Azure Multiimager

293   (Azure biosystems, Dublin, CA, USA).

294   *Analysis of E. coli growth*

295   *E. coli* mutant strains were cultivated in 750 µL MOPS minimal medium in a transparent 48-

296   well plate (Sarstedt, Nümbrecht, Germany) without or with supplementation of 5 mM GSH or

297   GSSG at 37 °C with continuous shaking in an infinite M200 multiplate reader (Tecan

298   instruments, Männedorf, Switzerland). Cells were inoculated to a starting OD_{600} of 0.1 and

299   bacterial growth was recorded every 30 min for 18 h.

14

300   **Results:**

301   *roGFP2 is completely oxidized in the E. coli periplasm, even in the absence of the major*

302   *oxidase DsbA*

303   The redox state of cellular compartments is often assessed by targeting genetically encoded

304   redox probes to the compartment of interest. One frequently used redox sensor is roGFP2, a

305   GFP variant, in which two cysteines were introduced at positions 147 and 204 that can form a

306   disulfide bond upon oxidation. This disulfide bond results in a shift in the fluorescence

307   excitation spectrum of the probe, in which the excitation maximum at 488 nm is reversibly

308   decreased with a simultaneous increase of the excitation peak at 405 nm. Excitation at either

309   maxima results in emission at ~510 nm. The ratio of the fluorescence emission intensity upon

310   excitation at 405 nm and 488 nm reflects changes in the dithiol disulfide state of the probe

311   and, in combination with fully oxidized and reduced controls, allows the determination of the

312   degree of the probe oxidation independent of probe concentration (Degrossoli et al., 2018;

313   Dooley et al., 2004; Lukyanov and Belousov, 2014; Meyer and Dick, 2010; Xie et al., 2020).

314   In order to assess the periplasmic oxidation state of *E. coli*, we targeted roGFP2 to this

315   compartment. GFP is usually not folding correctly in the periplasm, hence the general

316   secretory pathway (Sec) is unsuitable for targeting roGFP2 to the periplasm (Santini et al.,

317   2001). In contrast, *E. coli*'s twin-arginine translocase (or Tat system) transports completely

318   folded substrates over the inner membrane. Tat-translocation requires the presence of an N-

319   terminal signal peptide, characterized by an essential twin-arginine motif (Palmer and Berks,

320   2012; Thomas et al., 2001). To target roGFP2 to the periplasm via the Tat system, we

321   expressed the protein as an N-terminal torA$_{SS}$ fusion in the KEIO wildtype *E. coli* BW25113

322   (referred to as WT) (Baba et al., 2006) (Fig. 1A). We verified translocation of roGFP2 into

323   the periplasm using fluorescence microscopy (Fig. 1B, left panel). Determination of the

324   roGFP2 oxidation state (OxD) revealed complete oxidation of the probe in the periplasm of

15

325   *E. coli* WT (Fig. 1C, left panel). As the DsbA/DsbB pair is the major system for oxidative

326   protein folding in the periplasm of *E. coli* (Collet and Bardwell, 2002), roGFP2 was also

327   targeted to the periplasm of cells lacking DsbA (Fig. 1B, right panel). Surprisingly however,

328   periplasmic roGFP2 was still fully oxidized in the absence of DsbA (Fig. 1C, right panel),

329   suggesting the presence of an alternative mechanism for the introduction of disulfide bonds in

330   this compartment. In both cases, due to the complete oxidation of the probe, we were not able

331   to determine the redox potential for the roGFP2 dithiol disulfide couple.

332   *The redox-potential of the periplasm is significantly more reducing in cells lacking DsbA*

333   In order to determine the periplasmic redox potential exerted on proteins containing cysteines,

334   we turned to roGFP variants with a more oxidizing standard redox potential (Lohman and

335   Remington, 2008). These probes, termed roGFP-iX were developed by insertion of a single

336   amino acid (denoted by the 'X') adjacent to cysteine 147 resulting in a decreased stability of

337   the disulfide bond and midpoint potentials of –229 to –246 mV compared to –280 mV of

338   roGFP2. These roGFP-iX variants have been successfully used to monitor the oxidation state

339   of the endoplasmic reticulum, a highly oxidized compartment in eukaryotic cells and a major

340   site of oxidative protein folding (Delic et al., 2010; Dooley et al., 2004; Ugalde et al., 2022).

341   Thus, roGFP-iL with a midpoint potential of –229 mV was expressed and targeted to the

342   periplasm of the WT and Δ*dsbA* strain (Fig. 1A, B, right panel). In contrast to roGFP2,

343   roGFP-iL was only around 50 % oxidized in the WT periplasm (Fig. 1B, left panel), allowing

344   the calculation of the redox-potential using the Nernst equation as described before (Xie et al.,

345   2020). In the WT the redox-potential of roGFP-iL in the periplasm was –228 mV (Fig. 1E,

346   left panel). Not surprisingly, the lack of DsbA resulted in a more reduced roGFP-iL probe

347   (Fig. 1E, right panel). The shift in the redox-potential was around 14 mV to –243 mV,

348   supporting the role of DsbA in oxidative protein folding, however, the relatively small size of

16

349   the shift suggests the presence of an alternative mechanism for the introduction of disulfide

350   bonds.

351   *Periplasmic thiol oxidation is significantly impaired but not abrogated in a ΔdsbA-mutant*

352   Our experiments with roGFP2 and roGFP-iL reflected the steady state of thiol oxidation in the

353   periplasm. However, both stress and physiological situations are often accompanied by

354   increased protein secretion, requiring correct oxidative protein folding and hence, may affect

355   the redox homeostasis of the periplasm. In order to test the capacity of the periplasm to restore

356   its redox balance after reductive challenge, we evaluated the re-oxidation kinetics of
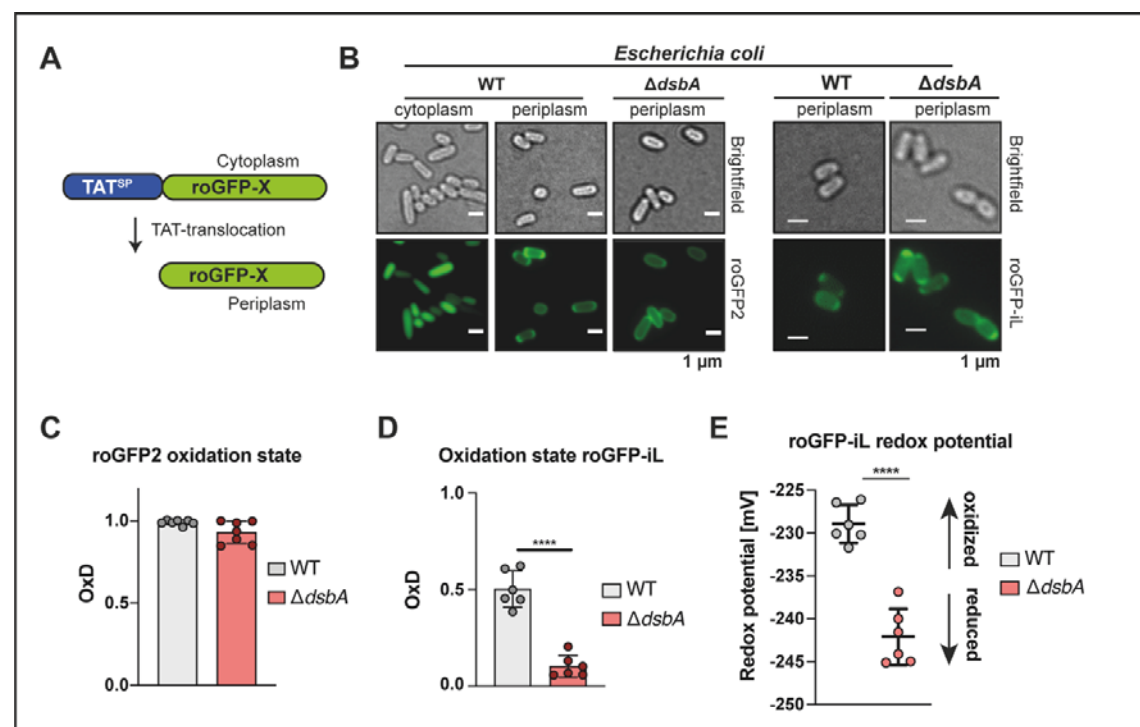

357

358   **Figure 1. Genetically encoded redox probes reveal the redox potential imposed onto thiol pairs the**
359   **periplasm of *E. coli*. (A)** Schematic depiction of the targeting of both roGFP probes to the periplasm by N-
360   terminal fusion with the torA signal sequence. **(B)** Correct localization of roGFP2 (left) and roGFP-iL
361   (right) is confirmed by fluorescence microscopy. **(C)** Oxidation state (OxD) of roGFP2 in the periplasm of
362   WT and cells lacking DsbA. The emission at 525 nm was recorded after excitation of roGFP2 at 488 nm
363   and 405 nm in *E. coli* WT or cells lacking DsbA. OxD was determined based on samples reduced with
364   DTT and oxidized with Aldrithiol-2 (AT-2). Each value represents the mean of three technical replicates.
365   Error bars represent the standard deviation in n=7 individual replicates. **(D)** Oxidation state (OxD) of
366   roGFP-iL in the periplasm of WT and of cells lacking DsbA. roGFP-iL emission at 525 nm was recorded
367   after excitation at 395 nm or 465 nm in *E. coli* WT or Δ*dsbA*. **(E)** The roGFP-iL redox potential was
368   calculated using the Nernst equation. Values were recorded in independent measurements and error bars
369   represent the standard deviation in n=6 individual replicates. Significance tests in B and C were performed
370   using Student's t-test ****$p<0.0001$.

17

371   periplasmic roGFP2 after a reductive pulse. To explore the role of DsbA in this process, we

372   also analyzed the re-oxidation of roGFP2 in cells lacking this oxidoreductase. In these

373   experiments, we treated WT and cells lacking DsbA cells, both expressing roGFP2 in the

374   periplasm with a pulse of DTT. This was followed by the removal of the reductant and the

375   recording of the oxidation state of roGFP2 over time (Fig. 2A). In the WT, periplasmic

376   roGFP2 oxidation starts immediately after DTT removal and restores maximum oxidation

377   within 150 min. Cells that lack DsbA also showed sensor re-oxidation, however, roGFP2 was

378   not restored to maximum oxidation in the time frame of our measurement (Fig. 2B).

379   Additionally, the re-oxidation rate, calculated as the linear slope after DTT removal, was

380   significantly lower in DsbA-deficient cells, however, there was still re-oxidation capacity

381   present (Fig. 2C). These findings suggest that there is an additional factor playing a role in

382   periplasmic redox homeostasis, other than DsbA. To further explore our hypothesis, we used

383   cell lysates derived from *E. coli* WT and DsbA-deficient cells and explored their capacity to

384   re-oxidize DTT-reduced, purified roGFP2 (Fig. 2D). Similar to the cell re-oxidation assay, we

385   calculated the oxidation rate from the linear slope within the first two hours of measurement.

386   Although roGFP2 oxidation by cell lysate was slow, when compared to intact cells, lysate

387   from WT was significantly faster in catalyzing roGFP2 re-oxidation than a Δ*dsbA* lysate.

388   However, in line with our previous findings, indicating another factor capable of catalyzing

389   disulfide bond formation in the periplasm, the Δ*dsbA* lysate was still significantly faster than a

390   buffer control (Fig. 2E, F). The rather slow oxidation of roGFP2 *in vitro* may be explained by

391   the fact that DsbA preferably introduces disulfide bonds in unfolded proteins entering the
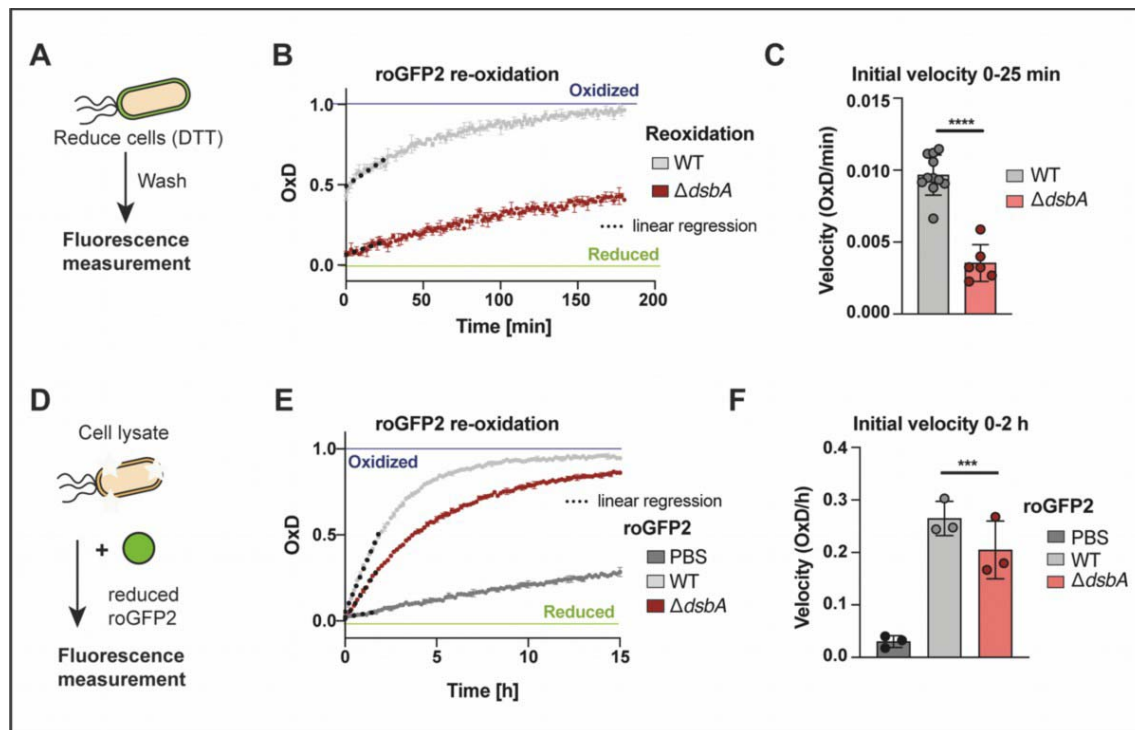
392   periplasm over folded ones (Kadokura et al., 2004).

393

Figure 2. Lack of the oxidase DsbA results in inhibited re-oxidation of roGFP2 *in vivo* and *in vitro*. **(A)** Schematic representation of the workflow of *in vivo* re-oxidation kinetics in the periplasm. **(B)** Re-oxidation of roGFP2 in the periplasm of *E. coli*. *E. coli* WT and Δ*dsbA*, expressing periplasmic roGFP2 were reduced with 10 mM DTT. The reductant was washed out and fluorescence intensities were recorded. DTT-reduced and AT-2-oxidized cells served as controls for calculation of OxD. One representative example out of at least six individual replicates is shown. Error bars represent standard deviation of the technical triplicates of that individual experiment. **(C)** For an estimation of the initial re-oxidation velocity, a linear regression was calculated for the first 25 min after start of the measurement (dashed lines in B). Values shown as circles are the mean of three technical repeats recorded in at least six independent experiments. Error bars reflect the standard deviation of the means. **(D)** Schematic representation of the workflow of *in vitro* re-oxidation kinetics using *E. coli* lysate. **(E)** Oxidation of purified roGFP2 by *E. coli* lysates. Purified roGFP2 was reduced with DTT, the reductant was removed and *E. coli* cell lysates of WT or Δ*dsbA* were added (10 µg of protein). One representative experiment is shown. Values displayed are the mean of three technical replicates. Error bars reflect the standard deviation. Note the different time scales in (B) and (E). **(F)** The initial re-oxidation velocity was calculated from a linear regression in the first 2 hours from the start of the measurement (dashed lines in E). Values (circles) are the mean of three technical replicates recorded in 3 independent measurements. Error bars reflect the standard deviation of the means. Significance tests in **(C)** were performed using Student's t-test and **(F)** using one way ANOVA. ***p< 0.001; ****p < 0.0001.

413   *Oxidized glutathione rescues periplasmic roGFP2 re-oxidation velocity in cells lacking DsbA*

414   Based on our observations, we suspected that glutathione (GSH) and its oxidized dimer GSSG

415   might influence the periplasmic redox balance in *E. coli* and thus might act as part of an

416   auxiliary system in oxidative folding. Glutathione is one of the most important redox-active

19

417   molecules inside many cells and it has been shown to be present in the periplasm (Eser et al.,

418   2009; Pittman et al., 2005).

419   We thus analyzed the periplasmic capacity for re-oxidizing roGFP2 in the presence of

420   glutathione after a reductive pulse. *E. coli* WT and DsbA-deficient cells producing

421   periplasmic roGFP2 were thus reduced with DTT, and, after reductant removal, roGFP2

422   oxidation was recorded in the presence of 5 mM GSH or GSSG (Fig. 3A). Surprisingly,

423   addition of GSH to WT cells resulted in an accelerated roGFP2 re-oxidation in the periplasm,

424   whereas GSSG supplementation had no discernible influence (Fig. 3B). In contrast, in cells

425   that lack DsbA, GSH and GSSG acted in a more expected way; while GSSG supplementation

426   rescued roGFP2 re-oxidation, GSH had no influence on the periplasmic redox dynamics in

427   Δ*dsbA* (Fig. 3C). Calculation of the re-oxidation rate confirmed that while GSH significantly

428   speeds up re-oxidation of periplasmic roGFP2 in the WT, GSSG significantly accelerates the

429   re-oxidation rate of roGFP2 in DsbA-deficient cells, essentially to WT level (Fig. 3D). Based

430   on these findings, we asked ourselves if DsbA is interacting with glutathione, causing the

431   observed opposite responses to GSH and GSSG in WT and DsbA-deficient *E. coli* cells.
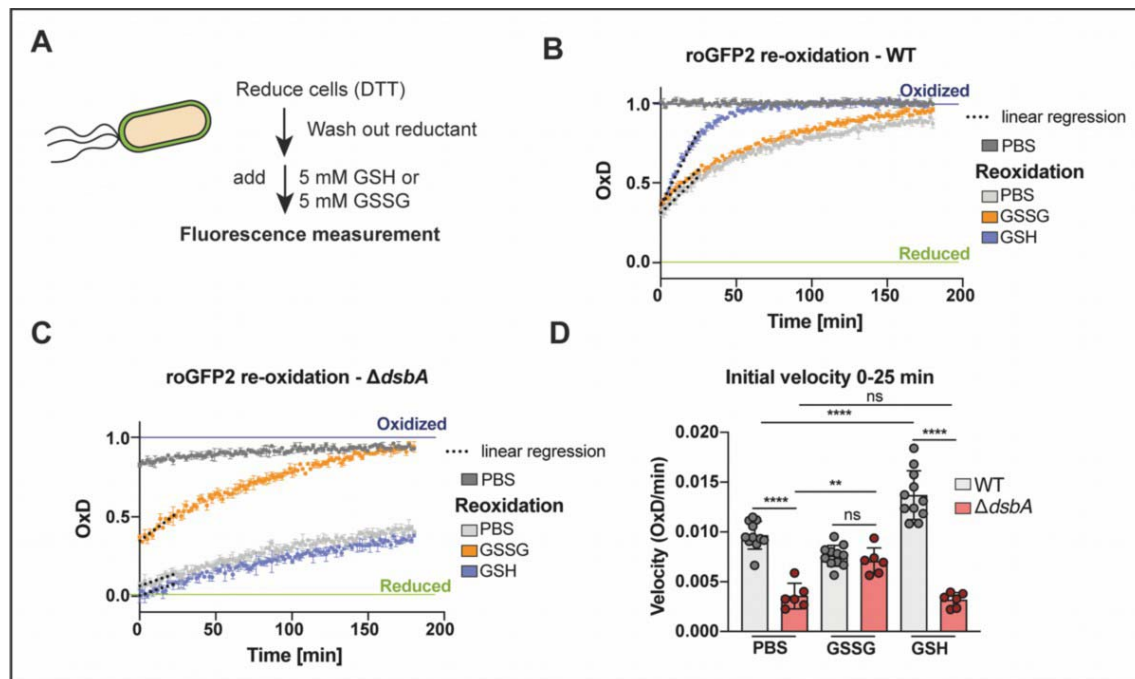
432

Figure 3. External addition of oxidized glutathione rescues the re-oxidation of roGFP2 in the periplasm of cells lacking DsbA, while reduced glutathione accelerates re-oxidation of roGFP2 in the periplasm of *E. coli* WT. (A) Schematic representation of the workflow of *in vivo* re-oxidation kinetics in the periplasm. *E. coli* WT **(B)** and Δ*dsbA* **(C)** expressing periplasmic roGFP2 were reduced with 10 mM DTT. The reductant was washed out, 5 mM GSH or GSSG were added and fluorescence intensities were recorded. DTT-reduced and AT-2-oxidized cells served as controls for calculation of OxD. A representative experiment is shown. Values are the mean of three technical replicates. Error bars reflect the standard deviation. **(D)** The initial re-oxidation velocity was calculated as linear regression for the first 25 min after start of the measurement (dashed lines in B and C). Values (circles) are the mean of three technical replicates recorded in a minimum of six experimentally independent replicates. Error bars represent the standard deviation. Values for PBS treated cells of the WT and Δ*dsbA* are the same as shown in Fig. 2 and are presented here for context. Significance test was performed using one way ANOVA. ns>0.05, **$p<0.01$, ****$p < 0.0001$.

Oxidized glutathione does not directly interact with the oxidase DsbA

To investigate if glutathione interacts with DsbA, we investigated the effect of GSSG on

DsbA-dependent roGFP2 oxidation *in vitro*. Purified DsbA was oxidized and added to

reduced roGFP2. Similar to the aforementioned lysate assay, the oxidation rate of roGFP2 by

DsbA is rather slow compared to *in vivo* re-oxidation, although significantly higher compared

to buffer alone (Fig. 4A, B). The oxidation rate of roGFP2 in the presence of GSSG alone was

slightly slower, but still comparable to roGFP2 oxidation by DsbA. Adding both GSSG and

21

453   DsbA at the same time did not even double the probe's oxidation rate, indicating an additive

454   effect of GSSG and DsbA and not a GSSG-driven catalytic action of DsbA.

455   To further confirm the incapability of DsbA to perform GSSG-dependent roGFP2 oxidation,

456   we used the cytosol of genetically manipulated yeast cells as "cellular test tubes". This assay

457   is performed in yeast cells, lacking the glutathione reductase (Glr1) and both cytosolic class I

458   dithiol glutaredoxins (Grx1, Grx2), while simultaneously expressing Opt1, a glutathione

459   transporter (Zimmermann et al., 2021). This *in vivo* system should enable us to monitor a

460   potential DsbA-catalyzed oxidation of roGFP2 by GSSG in the absence of any *E. coli*-specific

461   factors. For this, we engineered a roGFP2-DsbA fusion construct and expressed it in the

462   cytosol of the Δ*glr*Δ*grx*1Δ*grx*2 yeast cells, following the exogenous application of GSSG

463   concentrations between 1.5-100 μM. Unfused roGFP2 served as negative and roGFP2 fused

464   to *homo sapiens* glutaredoxin (roGFP2-*Hs*Grx) as positive control for direct interaction with

465   GSSG. In this assay, GSSG-driven roGFP2 oxidation did not depend on the oxidase DsbA

466   (Fig. 4C, D). However, we cannot exclude that roGFP2 is an inappropriate substrate of DsbA

467   in the fusion construct and therefore roGFP2 may not be oxidized by DsbA in this assay. In

468   contrast, the roGFP2-*Hs*Grx fusion probe strongly reacted to the addition of GSSG (Fig. 4E).

469   Both the *in vitro* and the "cellular test tube" approach strongly suggest that DsbA does not

470   interact with glutathione itself, indicating that the role of glutathione in the periplasmic redox

471   homeostasis is independent of the known mechanism for disulfide bond formation in *E. coli*.
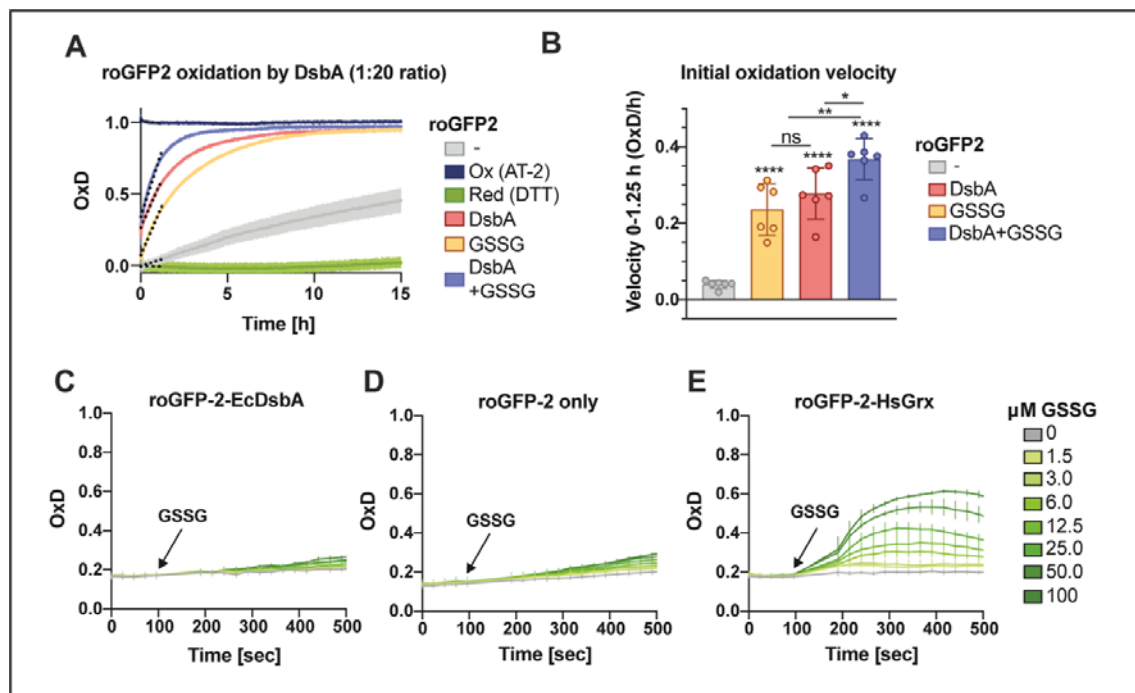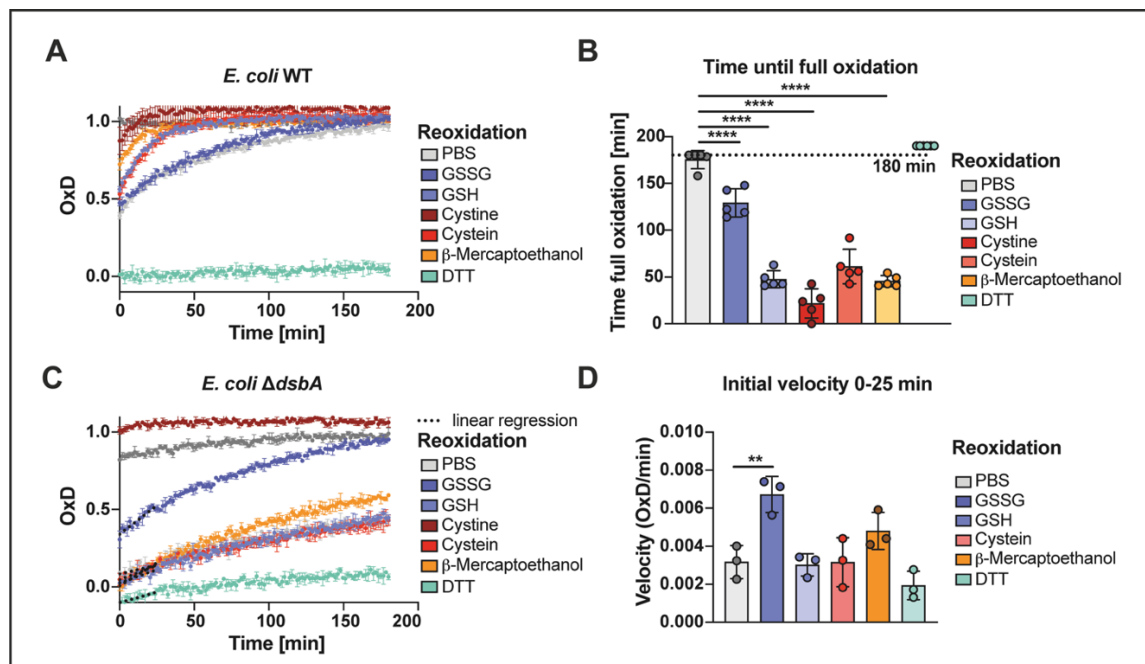
22

Figure 4. Oxidation of roGFP2 by oxidized glutathione (GSSG) is not catalyzed by DsbA. (A) Oxidation of purified reduced roGFP2 by AT-2-oxidized DsbA (red), GSSG (orange) or both (purple). Purified roGFP2 was reduced with DTT, the reductant was washed out and DsbA and/or GSSG were added in a 20-fold molar access. PBS was used to track air oxidation of roGFP2. DTT served as reduction and AT-2 as oxidation controls for calculation of OxD. **(B)** The initial re-oxidation velocity was calculated as linear regression for the first 1.25 hours after the start of measurement (dashed lines A). Values (circles) are the mean of three technical replicates recorded in a minimum of six independent repeats and error bars depict standard deviation. Significance test was performed using one-way ANOVA ns $p>0.05$ *$p<0.05$, **$p<0.01$, ***$p<0.001$, ****$p < 0.0001$. **(C)** The oxidation state of the cytosolic roGFP2 fusion protein roGFP2-*Ec*DsbA was monitored in ScOpt1/ScHgt1 YPH449 *glr1 grx1 grx2* yeast cells upon exogenous addition of different GSSG amounts. Unfused roGFP2 **(D)** served as negative and roGFP2-*Hs*Grx1 **(E)** as positive control for protein-GSSG interaction. Values **(B-E)** are the mean of four individual replicates and error bars depict the standard deviation.

Monothiols accelerate roGFP2 re-oxidation in a DsbA-dependent mechanism

While we excluded the interaction of GSSG with DsbA, we showed that the addition of GSH accelerated the re-oxidation rate of periplasmic roGFP2 after a reductive pulse in a DsbA-dependent manner (Fig. 3B, D). To investigate whether this effect is limited to GSH, we tested the influence of other reduced monothiols and dithiols. Cystein, β-mercaptoethanol, and DTT were added to *E. coli* WT and Δ*dsbA* cells and roGFP2 re-oxidation dynamics in the periplasm were measured as described above. The addition of the monothiols cysteine and β-mercaptoethanol to WT significantly accelerated roGFP2 oxidation similar to GSH, as

23

494   measured by the time after which the probe reached full oxidation. In contrast to monothiols,

495   addition of the dithiol DTT to WT completely inhibited roGFP2 re-oxidation. We also

496   included cystine in our assay, the oxidized form of the amino acid cysteine. In contrast to

497   GSSG, which had no impact on the roGFP2 oxidation rate in WT, cystine massively reduced

498   the time until full oxidation was reached (Fig. 5A, B). In the Δ*dsbA* mutant, the presence of

499   monothiols had no significant impact, while cystine supplementation caused a drastically

500   increased re-oxidation state and rate, similar to WT (Fig. 5C, D). Overall, these findings

501   suggest a DsbA-dependent effect of monothiols, accelerating thiol oxidation in the periplasm,

502   even though we did not observe direct interaction of oxidized glutathione with DsbA itself.

Figure 5. The re-oxidation of periplasmic roGFP2 in *E. coli* WT is accelerated by external addition of different monothiols. (A) Influence of monothiols on the re-oxidation of roGFP2 in *E. coli* periplasm after a reductive pulse. *E. coli* WT cells with roGFP2 in their periplasms were reduced with 10 mM DTT, before the reductant was washed out and 5 mM GSH, GSSG, cysteine, cystine, DTT or β-mercaptoethanol were added. Then, fluorescence intensities were recorded for 3 h. DTT-reduced and AT-2-oxidized cells served as controls for calculation of OxD. Values displayed are the mean of three technical replicates representative for five independent experiments. Error bars reflect the standard deviation. **(B)** The time after which roGFP2 was completely oxidized was calculated to visualize differences in the re-oxidation speed. Values (circles) are the mean of three technical replicates recorded in five independent measurements. DTT-treatment did not result in re-oxidation during the 180 min measurement time. Error bars reflect the standard deviation of the means. Significance test was performed using one way ANOVA. ****$p < 0.0001$. **(C)** Influence of monothiols on the re-oxidation of roGFP2 in the periplasm of *E. coli* cells lacking DsbA after a reductive pulse. Values shown are the mean of three technical replicates, representative for three independent experiments. Error bars depict the standard deviation. **(D)** The initial re-oxidation velocity was calculated as linear regression for the first 25 min after start of the measurement (dashed lines A). Values (circles) are the mean of three technical replicates recorded in three independent repeats and error bars depict the standard deviation of those means. Significance test in was performed using one-way ANOVA ns $p>0.05$, **$p<0.01$.

Endogenous glutathione is involved in stabilizing and maintaining the periplasmic redox state

All our experiments thus far were performed with exogenous glutathione. But we also

wondered about the role of endogenous glutathione, synthesized in *E. coli*'s cytoplasm. For

this, we determined the oxidation state of periplasmic roGFP-iL in cells lacking GshA, the

first enzyme of *E. coli*'s glutathione biosynthesis pathway. In glutathione-free media, these

cells do not contain GSH (Apontoweil and Berends, 1975; Carmel-Harel and Storz, 2000).

Confirming our observation with exogenous GSH, our experiment revealed a slightly, but

529   significantly lower oxidation of roGFP-iL in the periplasm of cells lacking GSH. The redox

530   potential shifted from around –228 mV (WT) to –233 mV, counterintuitively a more reducing

531   state, in the absence of GSH (Fig. 6A, B). Nevertheless, the shift was not as pronounced as in

532   cells lacking DsbA, which had a roGFP-iL redox potential of around –243 mV (Fig. 1E).

533   We also asked whether the presence of endogenous GSH leads to faster re-oxidation of

534   roGFP2. To address this question, we analyzed the capacity to restore the redox balance after

535   reductive challenge in GSH-depleted cells producing periplasmic roGFP2 as described before.

536   Our data indicates that roGFP2 oxidation rate and end oxidation state in the periplasm of

537   GSH-deficient cells was comparable to WT (Fig. 6C, D) suggesting GSH is not essential for

538   recovery after a reductive challenge.

539   Next, we asked what happens when both, DsbA and GSH are missing. The redox state of

540   roGFP-iL in a Δ*gshA*Δ*dsbA* strain showed a periplasmic redox potential imposed on the

541   sensor (ca. –244 mV) similar to the redox potential in the *dsbA* single mutant (ca. –243 mV)

542   (Fig. 1, Fig. 6B). Intriguingly however, using a Δ*gshA*Δ*dsbA* strain in a periplasmic roGFP2

543   re-oxidation assay revealed that exogenous GSSG did not completely restore WT oxidation

544   rate and final oxidation state (Fig. 6E, F) contrary to cells lacking solely DsbA (Fig. 3).

545   Adding GSH to a Δ*gshA*Δ*dsbA* strain even decelerated periplasmic roGFP2 oxidation,

546   something we did not observe in the Δ*dsbA* single mutant (Fig 3). These experiments indicate

547   that a fine-tuned balance of reduced and oxidized glutathione plays a role in stabilizing and

548   maintaining the redox environment in the periplasm of *E. coli*, and cells lacking both DsbA

549   and endogenous glutathione can neither fully utilize the oxidative power of exogenous GSSG

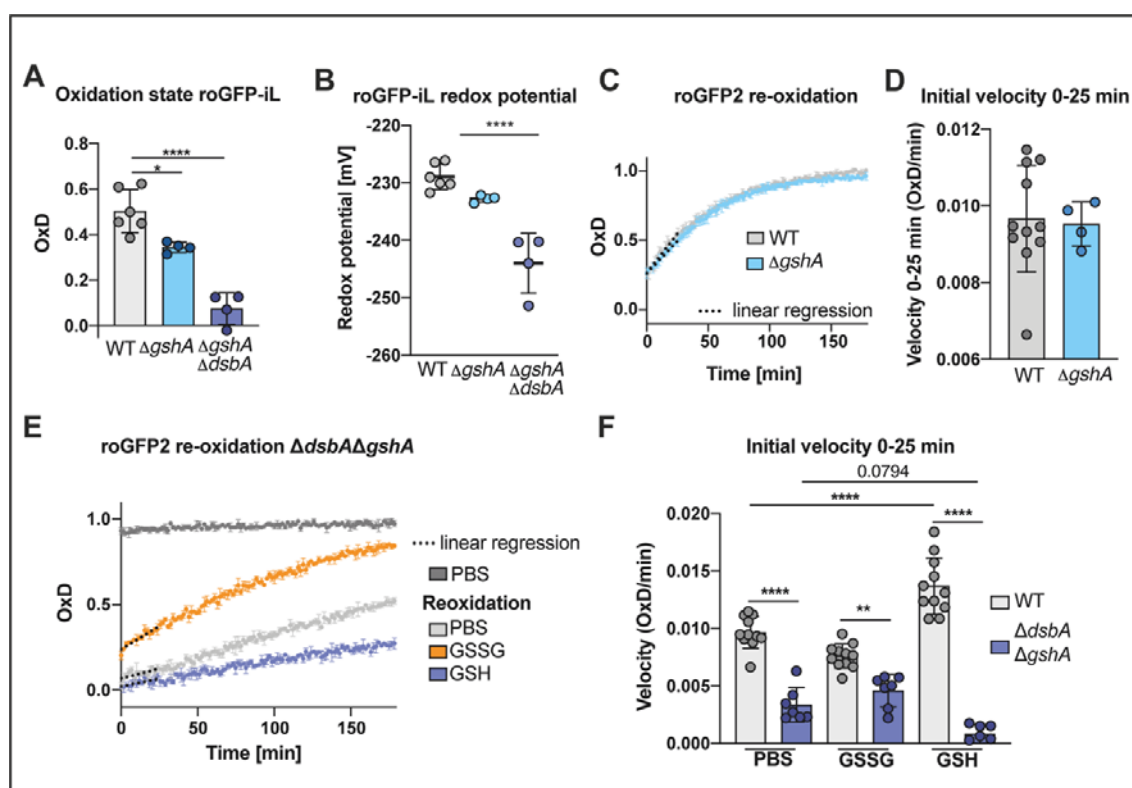550   nor compensate the reductive power of GSH in their periplasm.

Figure 6. Expression of roGFP probes in cells lacking DsbA and analysis of the periplasmic redox potential and re-oxidation rates indicate that endogenous glutathione is involved in stabilizing and maintaining the periplasmic redox state. (A) Oxidation state (OxD) of roGFP-iL in the periplasm of WT and cells lacking GSH. The emission at 525 nm was recorded after excitation at 395 nm or 465 nm of roGFP-iL in the respective cells. Oxidized or reduced roGFP-iL was generated by treatment of cells with AT-2 or DTT. **(B)** The periplasmic redox potential was calculated from (A) using the Nernst equation. The Values (circles) are the mean of three technical replicates recorded in a minimum of four independent repeats and error bars depict standard deviation of the means. Values for the WT were already shown in Fig. 2 and are presented again for context. Significance tests in A and B were performed using ANOVA-test. ****p<0.0001. **(C)** Re-oxidation of roGFP2 in the periplasm of *E. coli* WT and Δ*gshA*. The assay was performed as described in Fig. 2. One representative example out of at least four individual repeats is shown. Error bars represent standard deviation of technical triplicates. **(D)** The initial re-oxidation velocity was calculated from linear regression for the first 25 min after start of the measurement (dashed lines in B). Values shown as circles are the mean of three technical repeats recorded in at least four independent assays. **(E)** Re-oxidation of periplasmic roGFP2 in *E. coli* Δ*gshA*Δ*dsbA*. One representative example out of at least seven individual repeats is shown. Error bars represent standard deviation of technical triplicates. **(F)** The initial re-oxidation velocity was calculated from linear regression in the first 25 min after start of the measurement (dashed lines). Values (circles) are the mean of three technical replicates recorded in a minimum of seven independent repeats. Error bars represent the standard deviation. Significance test was performed using one way ANOVA. **p<0.01, ****p < 0.0001. Values for the WT were already shown in Fig. 3 and are presented again for context.

27

573   *Endogenous glutathione is involved in disulfide bond formation in E. coli's own periplasmic*

574   *proteins*

575   The observed influence of GSH on growth phenotypes (Supplementary figure 3) suggests that

576   our previous observations of disulfide bond formation in heterologously expressed roGFP-

577   based redox sensors also apply to endogenous DsbA substrates. One well-characterized

578   substrate of DsbA is alkaline phosphatase PhoA. PhoA is only active upon formation of

579   intramolecular disulfide bonds essential for correct protein folding. The activity of this

580   enzyme can be measured in a colorimetric assay using the substrate *para-*

581   nitrophenolphosphate (Fig. 7A) (Berg, 1981; Brickman and Beckwith, 1975; Sone et al.,

582   1997). We thus tested the activity of alkaline phosphatase PhoA in different *E. coli* deletion

583   strains grown in MOPS minimal medium. As described above, the lack of GSH, although

584   without effect on re-oxidation of roGFP2 in the periplasm, slightly shifted the periplasmic

585   redox homeostasis to more reducing conditions, as seen in the lowered redox potential of

586   roGFP-iL in those cells (Fig. 6). In accordance with this, PhoA activity was slightly, but

587   significantly lowered in GSH-deficient cells compared to WT. Also, in line with our previous

588   results (Fig. 1), cells lacking DsbA showed only poor PhoA activity, and the same was true

589   for cells lacking both DsbA and GSH (Fig. 7B).

590   To test whether the observed reduction in PhoA activity is dependent on glutathione levels in

591   the periplasm, we also measured PhoA activity in a *cydD* mutant. This mutant can still

592   synthesize glutathione, but is not able to produce the inner membrane ABC-transporter

593   CydDC that transports glutathione from the cytosol into the periplasm and hence suffers from

594   reduced periplasmic glutathione levels (Mironov et al., 2020; Pittman et al., 2005; Shepherd,

595   2015). Again, we observed a slight, but significant reduction of PhoA activity in this strain,

596   although less pronounced than in cells completely lacking glutathione biosynthesis (Fig. 7B).

597   Conversely, blocking glutathione transport from the periplasm into the cytosol by deleting

28

598   GsiC, the inner membrane component of the GsiA-D ABC Transporter (Suzuki et al., 2005;

599   Wang et al., 2017, 2018) did not result in significant changes in PhoA activity compared to

600   the WT.

601   Next, we supplemented the growth medium with exogenous GSSG to test if, in accordance

602   with the re-oxidation assays (Fig. 3) and the rescue of the growth phenotype (Supplementary

603   figure 3), it can assist in oxidative folding of PhoA in the absence of DsbA. Indeed, GSSG

604   addition restored PhoA activity back to WT level (Fig. 7C). Furthermore, addition of

605   exogenous GSSG also increased PhoA activity in the WT, contrary to what we observed with

606   roGFP2, suggesting that the role of periplasmic glutathione in oxidative folding differs,

607   depending on the protein in question (Fig. 3, Supplementary figure 3).

608   Proteins that are not correctly folded are usually unstable in the periplasm (Hiniker and

609   Bardwell, 2004), and thus no PhoA protein could be detected on a western blot in DsbA-

610   deficient cells (Fig. 7D). External GSSG addition prevented PhoA from degradation in a

611     $\Delta dsbA$ mutant.

612   Taken together, our data indicates a significant role for glutathione, not only in oxidative

613   protein folding of periplasmic proteins, but also by balancing and maintaining the periplasmic
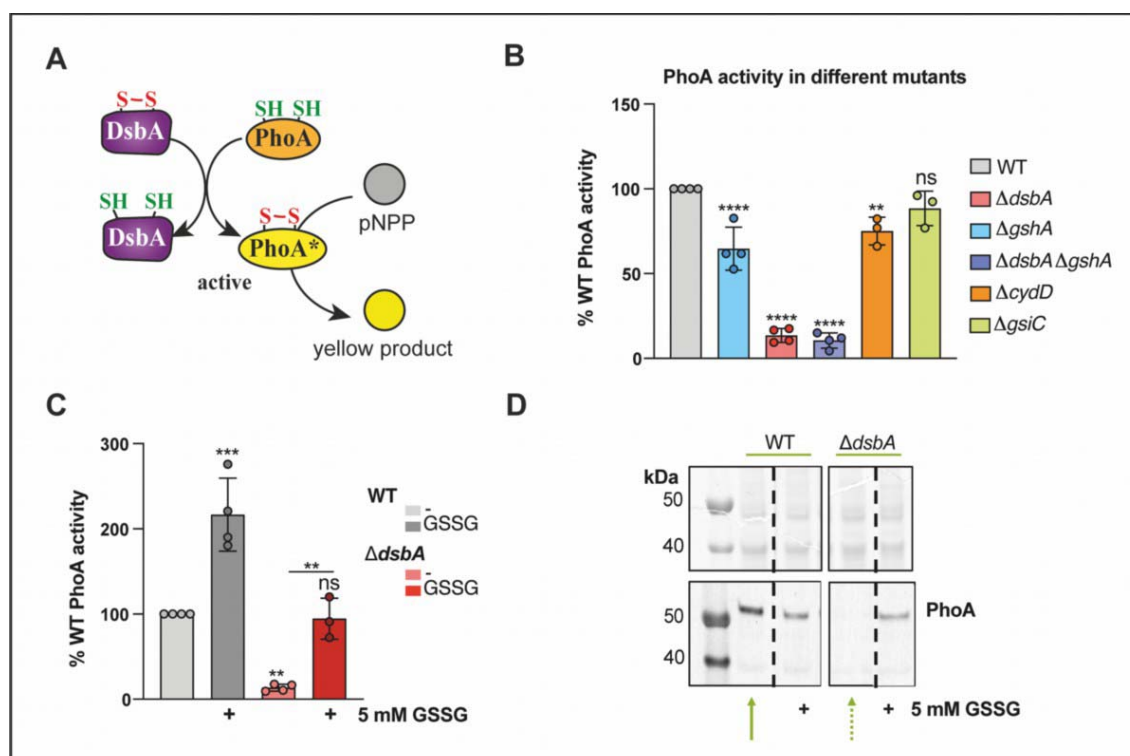
614   redox homeostasis.

Figure 7. Endogenous alkaline phosphatase (PhoA) is less active in the absence of glutathione and DsbA in the periplasm, and GSSG restores oxidative folding of PhoA in the absence of DsbA. (A) PhoA activity depends on oxidation by DsbA and activity of PhoA can be monitored using *p*-nitrophenylphosphate (pNPP) resulting in formation of the yellow product *p*-nitrophenol. **(B)** PhoA activity was assayed in cells cultivated in MOPS medium for 24 h at 37 °C. Release of *p*-nitrophenol from the PhoA substrate pNPP was measured and relative PhoA activity in % of WT activity was calculated. **(C)** GSSG restores PhoA activity to WT level in cells lacking DsbA. Cells were cultivated in MOPS medium in the presence of 5 mM GSSG for 18 h at 37 °C. Then fresh GSSG (5 mM) was added and the cells were incubated for 1 h. PhoA activity was assayed as described above. **(D)** PhoA accumulation was analyzed by SDS-PAGE and western blot in cells cultivated as described in **(C)**. For western blot a PhoA specific first and a fluorophore-coupled second antibody were used and fluorescence signal was scanned. Values in B and C are the mean of at least three independent replicates of duplicate assays with error bars representing the standard deviation. Significance test was performed using one way ANOVA. ns *p*>0.05 **p<0.05, ***p*<0.01, ***p<0.001, ****p < 0.0001.

630   **Discussion:**

631   The DsbA/B system is the major thiol oxidation system in the periplasm of *E. coli* and

632   together with the DsbC/D thiol disulfide isomerase system forms the oxidative folding

633   machinery (Collet and Bardwell, 2002; Manta et al., 2019). The standard redox potentials of

634   those systems are known (Wunderlich et al., 1993; Zapun et al., 1995), but the *in vivo* redox

635   potential seen by protein thiol disulfide pairs in the periplasm is unknown. Here, we used the

636   genetically encoded proteins roGFP2 and roGFP-iL targeted to the periplasm to directly probe

637   the thiol redox homeostasis in this compartment. When expressed in the cytosol of *E. coli*, the

638   probe roGFP2 with a midpoint redox potential of –280 mV is almost completely reduced

639   (Degrossoli et al., 2018). However, we found that it is virtually fully oxidized, when

640   expressed in the periplasm, suggesting that its engineered cysteine residues are completely

641   oxidized by the oxidative folding machinery.

642   To our surprise, roGFP2 was also fully oxidized in cells lacking the major thiol oxidase in the

643   periplasm, DsbA. We thus also analyzed the re-oxidation capacity after a reductive pulse, as

644   the oxidation state in an unperturbed cell solely reflects the steady state. And in the absence of

645   DsbA we did indeed find a significantly diminished re-oxidation velocity underlining the

646   importance of DsbA for oxidative folding.

647   Using roGFP-iL, we were able to determine that the redox potential imposed onto a thiol pair

648   in the periplasm is -229 mV. In the absence of DsbA, this redox potential shifted to a more

649   reducing -243 mV. In a previous study, Messens et al. used an Ag/AgCl electrode to measure

650   the redox potential in *E. coli* WT periplasmic extracts (Messens et al., 2007). Typically, an

651   electrode will measure the redox potential of all species it can chemically interact with and in

652   this case the redox potential was determined to be -165 mV. Unexpectedly, in their setting,

653   removal of DsbA shifted the redox potential to an even more oxidizing redox potential. Our

654   finding that the thiol disulfide redox potential is significantly below the overall redox

31

655   potential observed by Messens et al. with an electrode could explain their seemingly

656   paradoxical finding, since in a Δ*dsbA* strain a component that is reducing in comparison to the

657   overall redox potential measured by the electrode is removed from the overall redox pool. In

658   our case, removal of DsbA did indeed result in an overall more reducing redox potential

659   imposed on thiol pairs.

660   In concordance with our results in the periplasm, roGFP2 targeted to the ER is fully oxidized,

661   as well. Similarly, a roGFP2-iL-Grx1 fusion redox probe targeted to the ER of *Arabidopsis*

662   *thaliana* cells lacking Ero1/2, the functional homolog of DsbB in eukaryotes was more

663   reduced, and re-oxidation after a reductive pulse was inhibited by the lack of Ero1/2 (Ugalde

664   et al., 2022).

665   While roGFP2 re-oxidation was diminished in Δ*dsbA*, it was not absent, suggesting to us the

666   presence of an alternative pathway for disulfide bond formation. As glutathione is one of the

667   major redox buffers in cells, we assumed a possible role for the small molecule in periplasmic

668   redox homeostasis. Glutathione's cytosolic functions have been studied extensively and, until

669   a few years back, GSH was thought to be absent from the periplasm (Pittman et al., 2005).

670   However, relatively high glutathione levels in the periplasm of *E. coli* were discovered

671   recently, and since, there is an ongoing debate on its function in this compartment (Delaunay-

672   Moisan et al., 2017; Eser et al., 2009; Pittman et al., 2005). Interestingly, cells lacking the

673   transporter for GSH from the cytosol to the periplasm, CydDC, exhibit several phenotypes,

674   including DTT sensitivity and swarming defects, also found in cells deficient in oxidative

675   protein folding. This is an additional indication for a role of GSH in redox homeostasis and

676   oxidative folding in the periplasm. (Fabianek et al., 2000; Goldman et al., 1996; Pittman et al.,

677   2005; Smirnova et al., 2012). Accordingly, we found that re-oxidation of periplasmic roGFP2

678   in Δ*dsbA* was restored by the addition of exogenous GSSG, while it was not influenced in

679   WT. Surprisingly, adding exogenous GSH to the WT accelerated roGFP2 re-oxidation, but

680   not in a Δ*dsbA* strain. We also observed this seemingly paradoxical acceleration of thiol re-

32

681   oxidation in WT by other reducing monothiols like cysteine or β-mercaptoethanol. However,

682   we did not observe direct interactions of DsbA with glutathione *in vitro* and in our yeast cell

683   experiments.

684   We next assessed the role of endogenous glutathione in the redox balance of the periplasm.

685   And in line with our observations with exogenous GSH, the oxidation state of roGFP-iL was

686   slightly shifted to a more reducing state in Δ*gshA*, indicating a role for endogenous

687   glutathione in the periplasmic redox homeostasis as well. It should be noted, however, that

688   roGFP2 re-oxidation in a GSH-deficient mutant was comparable to WT. Taken together, the

689   presence of GSH and GSSG in the periplasm, driven by the availability of exogenous and

690   endogenous glutathione, seems to be important for the fine-tuning of the periplasmic redox

691   potential.

692   Expression of a non-native redox sensor might not reflect the natural redox state in the

693   periplasm or might even influence it by diverting oxidative power available for the formation

694   of native disulfide bonds. We thus analyzed the activity of PhoA, a native *E. coli* protein,

695   which depends on oxidation by DsbA for its activity, in different mutants. This approach

696   revealed that reduced periplasmic glutathione levels indeed resulted in significantly lower

697   PhoA activity, in line with the more reduced roGFP-iL redox state in Δ*gshA*. While PhoA's

698   oxidative folding is clearly influenced by the presence or absence of GSH, not all DsbA

699   substrates seem to be influenced by glutathione. RNaseI folding and isomerization by

700   DsbA/DsbC e.g., was not influenced by the loss of GSH (Messens et al., 2007).

701   In order to understand the role of glutathione in the periplasm, it is helpful to have a look at

702   the role of GSH in the eukaryotic ER, for which, in contrast to bacteria, more studies are

703   available. In the ER, the glutathione concentration is around 15 mM, higher than in whole cell

704   lysates with around 7 mM (Birk et al., 2013). Similar to the periplasm, the GSH:GSSG ratio

705   in the ER is lower (3:1 to 1:1) compared to the cytosol (100:1), resulting in a more oxidizing

706   environment (Hwang et al., 1992). It is discussed whether GSH is the reductive power for

707   disulfide isomerization by PDI (Vitu et al., 2010) and high GSSG levels could act as oxidant

708   reservoir; however, it is still unclear if GSSG itself is able to oxidize PDI (Lappi and

709   Ruddock, 2011; Ushioda and Nagata, 2019). In the periplasm of Gram-negative bacteria,

710   DsbB recycles DsbA, but in contrast to Ero1, it uses the respiratory chain as electron sink. As

711   aforementioned, we observed accelerated roGFP2 re-oxidation in the WT, but not in $\Delta dsbA$,

712   when adding monothiols to the cells and the opposite effect for GSSG, compensating the lack

713   of DsbA, raising the question whether DsbB is somehow regulated by glutathione. However,

714   analyzing a *dsbB* mutant strain regarding its oxidation state and re-oxidation capacity in

715   presence or absence of GSH or GSSG revealed that GSSG was still able to complement for

716   the loss of DsbB, indicating a DsbB-independent mechanism (Supplementary figure 4).

717   Overall, we showed that oxidized glutathione can compensate for the loss of DsbA by an

718   unknown mechanism. One possibility is that oxidized glutathione directly oxidizes roGFP2

719   and other reduced proteins, however previous studies (Müller et al., 2017) and the current *in*

720   *vitro* and yeast data show that direct roGFP2 oxidation by glutathione is very inefficient.

721   Another possibility is the presence of a yet unidentified redox factor in the periplasm that can

722   catalyze oxidative protein folding in the absence of DsbA. One possibility is DsbC and it has

723   been suggested that reduced glutathione can react with the isomerase, especially by providing

724   reductive power when DsbD is missing (Pittman et al., 2005; Smirnova et al., 2012).

725   However, (Messens et al., 2007) could also show that DsbC alone was not able to substitute

726   for DsbA in folding of RNaseI. In the ER up to 20 different oxidoreductases, for example the

727   peroxiredoxin Prx4 or the glutathione peroxidase-like enzymes Gpx7 and Gpx8 are found

728   besides PDI and for at least some of them it has been proposed that they possibly oxidize PDI

729   (Nguyen et al., 2011; Wang et al., 2018; Zito et al., 2010). We think it is possible, that *E. coli*

730   has a similar backup system for DsbA, presumably a glutaredoxin-like protein, which is

731   coupled to the periplasm's glutathione pool, providing either oxidizing or reducing power.

732   Taken together, our data underlines the importance of glutathione as a player in redox

733   homeostasis not only in the cytosol, but also in oxidative cellular compartments and it shows

734   that its role in oxidative protein folding did already evolve in bacteria.

Acknowledgements

Author contributions

LRK and LIL designed the study. LRK planned and performed most of the experiments. The yeast cell assays were designed and conducted by JZ and BM. JFS performed initial experiments, established the re-oxidation assay and constructed the pPT and pPT_*roGFP2* plasmids. NL and BC purified proteins and BC assisted with DsbA *in vitro* assays. LRK and LIL wrote the manuscript. All authors consulted on the manuscript and approved the final version.

Conflict of interest

The authors declare that they have no conflicts of interest with the contents of this article.

Funding

Data availability statement

The data supporting the findings of this study is presented within the article and its supplementary materials. Strains and plasmids constructed for this study are available upon request.

References

Ali Khan, H., Mutus, B., 2014. Protein disulfide isomerase a multifunctional protein with multiple physiological roles. Front. Chem. 2. https://doi.org/10.3389/fchem.2014.00070

Andersen, C.L., Matthey-Dupraz, A., Missiakas, D., Raina, S., 1997. A new *Escherichia coli* gene, *dsbG*, encodes a periplasmic protein involved in disulphide bond formation, required for recycling DsbA/DsbB and DsbC redox proteins. Mol. Microbiol. 26, 121–132. https://doi.org/10.1046/j.1365-2958.1997.5581925.x

Apontoweil, P., Berends, W., 1975. Isolation and initial characterization of glutathione-deficient mutants of Escherichia coli K 12. Biochim. Biophys. Acta BBA - Gen. Subj. 399, 10–22. https://doi.org/10.1016/0304-4165(75)90206-8

Aslund, F., Ehn, B., Miranda-Vizuete, A., Pueyo, C., Holmgren, A., 1994. Two additional glutaredoxins exist in *Escherichia coli*: glutaredoxin 3 is a hydrogen donor for ribonucleotide reductase in a thioredoxin/glutaredoxin 1 double mutant. Proc. Natl. Acad. Sci. 91, 9813–9817. https://doi.org/10.1073/pnas.91.21.9813

Åslund, F., Zheng, M., Beckwith, J., Storz, G., 1999. Regulation of the OxyR transcription factor by hydrogen peroxide and the cellular thiol—disulfide status. Proc. Natl. Acad. Sci. 96, 6161–6165. https://doi.org/10.1073/pnas.96.11.6161

Baba, T., Ara, T., Hasegawa, M., Takai, Y., Okumura, Y., Baba, M., Datsenko, K.A., Tomita, M., Wanner, B.L., Mori, H., 2006. Construction of *Escherichia coli* K-12 in-frame, single-gene knockout mutants: the Keio collection. Mol. Syst. Biol. 2, 2006.0008. https://doi.org/10.1038/msb4100050

Bardwell, J.C., Lee, J.O., Jander, G., Martin, N., Belin, D., Beckwith, J., 1993. A pathway for disulfide bond formation *in vivo*. Proc. Natl. Acad. Sci. 90, 1038–1042. https://doi.org/10.1073/pnas.90.3.1038

Bardwell, J.C.A., McGovern, K., Beckwith, J., 1991. Identification of a protein required for disulfide bond formation *in vivo*. Cell 67, 581–589. https://doi.org/10.1016/0092-8674(91)90532-4

Berg, P.E., 1981. Cloning and characterization of the *Escherichia coli* gene coding for alkaline phosphatase. J. Bacteriol. 146, 660–667. https://doi.org/10.1128/jb.146.2.660-667.1981

Birk, J., Meyer, M., Aller, I., Hansen, H.G., Odermatt, A., Dick, T.P., Meyer, A.J., Appenzeller-Herzog, C., 2013. Endoplasmic reticulum: reduced and oxidized glutathione revisited. J. Cell Sci. 126, 1604–1617. https://doi.org/10.1242/jcs.117218

Brickman, E., Beckwith, J., 1975. Analysis of the regulation of *Escherichia coli* alkaline phosphatase synthesis using deletions and φ80 transducing phages. J. Mol. Biol. 96, 307–316. https://doi.org/10.1016/0022-2836(75)90350-2

Carmel-Harel, O., Storz, G., 2000. Roles of the glutathione- and thioredoxin-dependent reduction systems in the *Escherichia coli* and *Saccharomyces cerevisiae* Responses to Oxidative Stress. Annu. Rev. Microbiol. 54, 439–461. https://doi.org/10.1146/annurev.micro.54.1.439

Cho, S.-H., Collet, J.-F., 2013. Many roles of the bacterial envelope reducing pathways. Antioxid. Redox Signal. 18, 1690–1698. https://doi.org/10.1089/ars.2012.4962

Christensen, S., Grøftehauge, M.K., Byriel, K., Huston, W.M., Furlong, E., Heras, B., Martin, J.L., McMahon, R.M., 2016. Structural and biochemical characterization of *Chlamydia trachomatis* DsbA reveals a cysteine-rich and weakly oxidising oxidoreductase. PLOS ONE 11, 1–22. https://doi.org/10.1371/journal.pone.0168485

Collet, J.-F., Bardwell, J.C.A., 2002. Oxidative protein folding in bacteria. Mol. Microbiol. 44, 1–8. https://doi.org/10.1046/j.1365-2958.2002.02851.x

804   Degrossoli, A., Müller, A., Xie, K., Schneider, J.F., Bader, V., Winklhofer, K.F., Meyer, A.J.,
805   Leichert, L.I., 2018. Neutrophil-generated HOCl leads to non-specific thiol oxidation
806   in phagocytized bacteria. eLife 7, e32288. https://doi.org/10.7554/eLife.32288
807   Delaunay-Moisan, A., Ponsero, A., Toledano, M.B., 2017. Reexamining the function of
808   glutathione in oxidative protein folding and secretion. Antioxid. Redox Signal. 27,
809   1178–1199. https://doi.org/10.1089/ars.2017.7148
810   Delic, M., Mattanovich, D., Gasser, B., 2010. Monitoring intracellular redox conditions in the
811   endoplasmic reticulum of living yeasts. FEMS Microbiol. Lett. 306, 61–66.
812   https://doi.org/10.1111/j.1574-6968.2010.01935.x
813   Dooley, C.T., Dore, T.M., Hanson, G.T., Jackson, W.C., Remington, S.J., Tsien, R.Y., 2004.
814   Imaging dynamic redox changes in mammalian cells with green fluorescent protein
815   indicators. J. Biol. Chem. 279, 22284–22293. https://doi.org/10.1074/jbc.M312847200
816   Eser, M., Masip, L., Kadokura, H., Georgiou, G., Beckwith, J., 2009. Disulfide bond
817   formation by exported glutaredoxin indicates glutathione's presence in the *E. coli*
818   periplasm. Proc. Natl. Acad. Sci. 106, 1572–1577.
819   https://doi.org/10.1073/pnas.0812596106
820   Fabianek, R.A., Hennecke, H., Thöny-Meyer, L., 2000. Periplasmic protein thiol:disulfide
821   oxidoreductases of *Escherichia coli*. FEMS Microbiol. Rev. 24, 303–316.
822   https://doi.org/10.1016/S0168-6445(00)00028-0
823   Fahey, R.C., Brown, W.C., Adams, W.B., Worsham, M.B., 1978. Occurrence of glutathione
824   in bacteria. J. Bacteriol. 133, 1126–1129. https://doi.org/10.1128/jb.133.3.1126-
825   1129.1978
826   Goldman, B.S., Gabbert, K.K., Kranz, R.G., 1996. The temperature-sensitive growth and
827   survival phenotypes of *Escherichia coli cydDC* and *cydAB* strains are due to
828   deficiencies in cytochrome bd and are corrected by exogenous catalase and reducing
829   agents. J. Bacteriol. 178, 6348–6351. https://doi.org/10.1128/jb.178.21.6348-
830   6351.1996
831   Greer, S., Perham, R.N., 1986. Glutathione reductase from *Escherichia coli*: cloning and
832   sequence analysis of the gene and relationship to other flavoprotein disulfide
833   oxidoreductases. Biochemistry 25, 2736–2742. https://doi.org/10.1021/bi00357a069
834   Gutscher, M., Pauleau, A.-L., Marty, L., Brach, T., Wabnitz, G.H., Samstag, Y., Meyer, A.J.,
835   Dick, T.P., 2008. Real-time imaging of the intracellular glutathione redox potential.
836   Nat. Methods 5, 553–559. https://doi.org/10.1038/nmeth.1212
837   Hiniker, A., Bardwell, J.C.A., 2004. *In vivo* substrate specificity of periplasmic disulfide
838   oxidoreductases *. J. Biol. Chem. 279, 12967–12973.
839   https://doi.org/10.1074/jbc.M311391200
840   Holyoake, L.V., Hunt, S., Sanguinetti, G., Cook, G.M., Howard, M.J., Rowe, M.L., Poole,
841   R.K., Shepherd, M., 2016. CydDC-mediated reductant export in *Escherichia coli*
842   controls the transcriptional wiring of energy metabolism and combats nitrosative
843   stress. Biochem. J. 473, 693–701. https://doi.org/10.1042/BJ20150536
844   Hwang, C., Sinskey, A.J., Lodish, H.F., 1992. Oxidized redox state of glutathione in the
845   endoplasmic reticulum. Science 257, 1496–1502.
846   https://doi.org/10.1126/science.1523409
847   Inaba, K., Ito, K., 2008. Structure and mechanisms of the DsbB–DsbA disulfide bond
848   generation machine. Biochim. Biophys. Acta BBA - Mol. Cell Res. 1783, 520–529.
849   https://doi.org/10.1016/j.bbamcr.2007.11.006
850   Inaba, K., Murakami, S., Nakagawa, A., Iida, H., Kinjo, M., Ito, K., Suzuki, M., 2009.
851   Dynamic nature of disulphide bond formation catalysts revealed by crystal structures
852   of DsbB. EMBO J. 28, 779–791. https://doi.org/10.1038/emboj.2009.21
853   Kadokura, H., Tian, H., Zander, T., Bardwell, J.C.A., Beckwith, J., 2004. Snapshots of DsbA
854   in action: detection of proteins in the process of oxidative folding. Science 303, 534–

855   537. https://doi.org/10.1126/science.1091724
856   Lappi, A.-K., Ruddock, L.W., 2011. Reexamination of the role of interplay between
857   glutathione and protein disulfide isomerase. J. Mol. Biol. 409, 238–249.
858   https://doi.org/10.1016/j.jmb.2011.03.024
859   Lohman, J.R., Remington, S.J., 2008. Development of a family of redox-sensitive green
860   fluorescent protein indicators for use in relatively oxidizing subcellular environments.
861   Biochemistry 47, 8678–8688. https://doi.org/10.1021/bi800498g
862   Lukyanov, K.A., Belousov, V.V., 2014. Genetically encoded fluorescent redox sensors.
863   Biochim. Biophys. Acta BBA - Gen. Subj. 1840, 745–756.
864   https://doi.org/10.1016/j.bbagen.2013.05.030
865   Manta, B., Boyd, D., Berkmen, M., 2019. Disulfide Bond Formation in the Periplasm of
866   *Escherichia coli*. EcoSal Plus 8. https://doi.org/10.1128/ecosalplus.ESP-0012-2018
867   Martin, J.L., Bardwell, J.C.A., Kuriyan, J., 1993. Crystal structure of the DsbA protein
868   required for disulphide bond formation *in vivo*. Nature 365, 464–468.
869   https://doi.org/10.1038/365464a0
870   Masip, L., Veeravalli, K., Georgiou, G., 2006. The many faces of glutathione in bacteria.
871   Antioxid. Redox Signal. 8, 753–762. https://doi.org/10.1089/ars.2006.8.753
872   Meister, A., 1988. Glutathione metabolism and its selective modification. J Biol Chem. 1988
873   Nov 25;263(33):17205-8. PMID: 3053703. J. Biol. Chem. Chem 25.
874   Messens, J., Collet, J.-F., Belle, K.V., Brosens, E., Loris, R., Wyns, L., 2007. The oxidase
875   DsbA folds a protein with a nonconsecutive disulfide. J. Biol. Chem. 282, 31302–
876   31307. https://doi.org/10.1074/jbc.M705236200
877   Meyer, A.J., Dick, T.P., 2010. Fluorescent protein-based redox probes. Antioxid. Redox
878   Signal. 13, 621–650. https://doi.org/10.1089/ars.2009.2948
879   Mironov, A., Seregina, T., Shatalin, K., Nagornykh, M., Shakulov, R., Nudler, E., 2020.
880   CydDC functions as a cytoplasmic cystine reductase to sensitize *Escherichia coli* to
881   oxidative stress and aminoglycosides. Proc. Natl. Acad. Sci. 117, 23565–23570.
882   https://doi.org/10.1073/pnas.2007817117
883   Missiakas, D., Georgopoulos, C., Raina, S., 1994. The *Escherichia colidsbC (xprA)* gene
884   encodes a periplasmic protein involved in disulfide bond formation. EMBO J. 13,
885   2013–2020. https://doi.org/10.1002/j.1460-2075.1994.tb06471.x
886   Missiakas, D., Georgopoulos, C., Raina, S., 1993. Identification and characterization of the
887   *Escherichia coli* gene *dsbB*, whose product is involved in the formation of disulfide
888   bonds *in vivo*. Proc. Natl. Acad. Sci. 90, 7084–7088.
889   https://doi.org/10.1073/pnas.90.15.7084
890   Müller, A., Schneider, J.F., Degrossoli, A., Lupilova, N., Dick, T.P., Leichert, L.I., 2017.
891   Systematic *in vitro* assessment of responses of roGFP2-based probes to
892   physiologically relevant oxidant species. Free Radic. Biol. Med. 106, 329–338.
893   https://doi.org/10.1016/j.freeradbiomed.2017.02.044
894   Nguyen, V.D., Saaranen, M.J., Karala, A.-R., Lappi, A.-K., Wang, L., Raykhel, I.B., Alanen,
895   H.I., Salo, K.E.H., Wang, C., Ruddock, L.W., 2011. Two endoplasmic reticulum PDI
896   peroxidases increase the efficiency of the use of peroxide during disulfide bond
897   formation. J. Mol. Biol. 406, 503–515. https://doi.org/10.1016/j.jmb.2010.12.039
898   Nilewski, S., Varatnitskaya, M., Masuch, T., Kusnezowa, A., Gellert, M., Baumann, A.F.,
899   Lupilov, N., Kusnezow, W., Koch, M.-H., Eisenacher, M., Berkmen, M., Lillig, C.H.,
900   Leichert, L.I., 2021. Functional metagenomics of the thioredoxin superfamily. J. Biol.
901   Chem. 296. https://doi.org/10.1074/jbc.RA120.016350
902   Palmer, T., Berks, B.C., 2012. The twin-arginine translocation (Tat) protein export pathway.
903   Nat. Rev. Microbiol. 10, 483–496. https://doi.org/10.1038/nrmicro2814
904   Pittman, M.S., Robinson, H.C., Poole, R.K., 2005. A bacterial glutathione transporter
905   (*Escherichia coli* CydDC) exports reductant to the periplasm. J. Biol. Chem. 280,

906   32254–32261. https://doi.org/10.1074/jbc.M503075200

907 Rietsch, A., Bessette, P., Georgiou, G., Beckwith, J., 1997. Reduction of the periplasmic
908   disulfide bond isomerase, DsbC, occurs by passage of electrons from cytoplasmic
909   thioredoxin. J. Bacteriol. 179, 6602–6608. https://doi.org/10.1128/jb.179.21.6602-
910   6608.1997

911 Santini, C.-L., Bernadac, A., Zhang, M., Chanal, A., Ize, B., Blanco, C., Wu, L.-F., 2001.
912   Translocation of jellyfish green fluorescent protein via the Tat system of *Escherichia*
913   *coli* and change of its periplasmic localization in response to osmotic Up-shock. J.
914   Biol. Chem. 276, 8159–8164. https://doi.org/10.1074/jbc.C000833200

915 Schneider, C.A., Rasband, W.S., Eliceiri, K.W., 2012. NIH Image to ImageJ: 25 years of
916   image analysis. Nat. Methods 9, 671–675. https://doi.org/10.1038/nmeth.2089

917 Shepherd, M., 2015. The CydDC ABC transporter of *Escherichia coli*: new roles for a
918   reductant efflux pump. Biochem. Soc. Trans. 43, 908–912.
919   https://doi.org/10.1042/BST20150098

920 Shevchik, V.E., Condemine, G., Robert-Baudouy, J., 1994. Characterization of DsbC, a
921   periplasmic protein of *Erwinia chrysanthemi* and *Escherichia coli* with disulfide
922   isomerase activity. EMBO J. 13, 2007–2012. https://doi.org/10.1002/j.1460-
923   2075.1994.tb06470.x

924 Smirnova, G., Muzyka, N., Oktyabrsky, O., 2012. Transmembrane glutathione cycling in
925   growing *Escherichia coli* cells. Microbiol. Res. 167, 166–172.
926   https://doi.org/10.1016/j.micres.2011.05.005

927 Smirnova, G.V., Muzyka, N.G., Oktyabrsky, O.N., 2005. Effects of cystine and hydrogen
928   peroxide on glutathione status and expression of antioxidant genes in *Escherichia coli*.
929   Biochem. Mosc. 70, 926–934. https://doi.org/10.1007/s10541-005-0204-2

930 Smirnova, G.V., Oktyabrsky, O.N., 2005. Glutathione in bacteria. Biochem. Mosc. 70, 1199–
931   1211. https://doi.org/10.1007/s10541-005-0248-3

932 Smirnova, G.V., Tyulenev, A.V., Muzyka, N.G., Oktyabrsky, O.N., 2020. Study of the
933   relationship between extracellular superoxide and glutathione production in batch
934   cultures of *Escherichia coli*. Res. Microbiol. 171, 301–310.
935   https://doi.org/10.1016/j.resmic.2020.07.004

936 Sone, M., Akiyama, Y., Ito, K., 1997. Differential *in vivo* roles played by DsbA and DsbC in
937   the formation of protein disulfide bonds*. J. Biol. Chem. 272, 10349–10352.
938   https://doi.org/10.1074/jbc.272.16.10349

939 Song, Y., Zhou, Z., Gu, J., Yang, J., Deng, J., 2021. Reducing the periplasmic glutathione
940   content makes *Escherichia coli* resistant to trimethoprim and other antimicrobial
941   drugs. Microbiol. Spectr. 9, e00743-21. https://doi.org/10.1128/Spectrum.00743-21

942 Suzuki, H., Koyanagi, T., Izuka, S., Onishi, A., Kumagai, H., 2005. The *yliA*, *-B*, *-C*, and *-D*
943   Genes of *Escherichia coli* K-12 Encode a Novel Glutathione Importer with an ATP-
944   Binding Cassette. J. Bacteriol. 187, 5861–5867.
945   https://doi.org/10.1128/JB.187.17.5861-5867.2005

946 Thomas, J.D., Daniel, R.A., Errington, J., Robinson, C., 2001. Export of active green
947   fluorescent protein to the periplasm by the twin-arginine translocase (Tat) pathway in
948   *Escherichia coli*. Mol. Microbiol. 39, 47–53. https://doi.org/10.1046/j.1365-
949   2958.2001.02253.x

950 Thomason, L.C., Costantino, N., Court, D.L., 2007. *E. coli* Genome Manipulation by P1
951   Transduction. Curr. Protoc. Mol. Biol. 79, 1.17.1-1.17.8.
952   https://doi.org/10.1002/0471142727.mb0117s79

953 Tu, B.P., Weissman, J.S., 2004. Oxidative protein folding in eukaryotes mechanisms and
954   consequences. J. Cell Biol. 164, 341–346. https://doi.org/10.1083/jcb.200311055

955 Tuggle, C.K., Fuchs, J.A., 1985. Glutathione reductase is not required for maintenance of
956   reduced glutathione in *Escherichia coli* K-12. J. Bacteriol. 162, 448–450.

40

957   https://doi.org/10.1128/jb.162.1.448-450.1985

958   Ugalde, J.M., Aller, I., Kudrjasova, L., Schmidt, R.R., Schlößer, M., Homagk, M., Fuchs, P.,
959   Lichtenauer, S., Schwarzländer, M., Müller-Schüssele, S.J., Meyer, A.J., 2022.
960   Endoplasmic reticulum oxidoreductin provides resilience against reductive stress and
961   hypoxic conditions by mediating luminal redox dynamics. Plant Cell 34, 4007–4027.
962   https://doi.org/10.1093/plcell/koac202

963   Ushioda, R., Nagata, K., 2019. Redox-mediated regulatory mechanisms of endoplasmic
964   reticulum homeostasis. Cold Spring Harb. Perspect. Biol. 11, a033910.

965   Vitu, E., Kim, S., Sevier, C.S., Lutzky, O., Heldman, N., Bentzur, M., Unger, T., Yona, M.,
966   Kaiser, C.A., Fass, D., 2010. Oxidative activity of yeast Ero1p on protein disulfide
967   isomerase and related oxidoreductases of the endoplasmic reticulum. J. Biol. Chem.
968   285, 18155–18165. https://doi.org/10.1074/jbc.M109.064931

969   Vivian, J.P., Scoullar, J., Rimmer, K., Bushell, S.R., Beddoe, T., Wilce, M.C.J., Byres, E.,
970   Boyle, T.P., Doak, B., Simpson, J.S., Graham, B., Heras, B., Kahler, C.M., Rossjohn,
971   J., Scanlon, M.J., 2009. Structure and function of the oxidoreductase DsbA1 from
972   *Neisseria meningitidis*. J. Mol. Biol. 394, 931–943.
973   https://doi.org/10.1016/j.jmb.2009.09.065

974   Wang, Z., Xia, X., Zhang, Meixian, Fang, J., Li, Y., Zhang, Meng, 2018. Purification and
975   Characterization of Glutathione Binding Protein GsiB from Escherichia coli. BioMed
976   Res. Int. 2018, 3429569. https://doi.org/10.1155/2018/3429569

977   Wunderlich, M., Glockshuber, R., 1993. In vivo control of redox potential during protein
978   folding catalyzed by bacterial protein disulfide-isomerase (DsbA). J. Biol. Chem. 268,
979   24547–24550. https://doi.org/10.1016/S0021-9258(19)74500-1

980   Wunderlich, M., Jaenicke, R., Glockshuber, R., 1993. The redox properties of protein
981   disulfide isomerase (DsbA) of *Escherichia coli* result from a tense conformation of its
982   oxidized form. J. Mol. Biol. 233, 559–566. https://doi.org/10.1006/jmbi.1993.1535

983   Xie, K., Varatnitskaya, M., Maghnouj, A., Bader, V., Winklhofer, K.F., Hahn, S., Leichert,
984   L.I., 2020. Activation leads to a significant shift in the intracellular redox homeostasis
985   of neutrophil-like cells. Redox Biol. 28, 101344.
986   https://doi.org/10.1016/j.redox.2019.101344

987   Zapun, A., Missiakas, D., Raina, S., Creighton, T.E., 1995. Structural and functional
988   characterization of DsbC, a protein involved in disulfide bond formation in
989   *Escherichia coli*. Biochemistry 34, 5075–5089. https://doi.org/10.1021/bi00015a019

990   Zechmann, B., Liou, L.-C., Koffler, B.E., Horvat, L., Tomašić, A., Fulgosi, H., Zhang, Z.,
991   2011. Subcellular distribution of glutathione and its dynamic changes under oxidative
992   stress in the yeast *Saccharomyces cerevisiae*. FEMS Yeast Res. 11, 631–642.
993   https://doi.org/10.1111/j.1567-1364.2011.00753.x

994   Zimmermann, J., Oestreicher, J., Geissel, F., Deponte, M., Morgan, B., 2021. An intracellular
995   assay for activity screening and characterization of glutathione-dependent
996   oxidoreductases. Free Radic. Biol. Med. 172, 340–349.
997   https://doi.org/10.1016/j.freeradbiomed.2021.06.016

998   Zito, E., Melo, E.P., Yang, Y., Wahlander, Å., Neubert, T.A., Ron, D., 2010. Oxidative
999   protein folding by an endoplasmic reticulum-localized peroxiredoxin. Mol. Cell 40,
1000   787–797. https://doi.org/10.1016/j.molcel.2010.11.010

1001   **Supplementary material**

1002   **Supplementary table 1. Bacterial and yeast strains used in this study**.

Strain	Relevant characteristics	Reference
E. coli strains		
DH5α	Cloning host	(Taylor et al., 1993)
BL21 (DE3)	Expression host	(Studier and Moffatt, 1986)
MG1655	Expression host	(Blattner et al., 1997)
E. coli KEIO strains		
WT (BW25113)	Δ(*araD-araB*)567, Δ*lacZ*4787(::*rrnB*-3), λ-, *rph*-1, Δ(*rhaD-rhaB*)568, *hsdR*514	(Baba et al., 2006)
Δ*gshA* (JW2663)	BW25113; Δ*gshA*769::km	
Δ*dsbA* (JW3832)	BW25113; Δ*dsbA*723::km	
Δ*gshA*Δ*dsbA*	BW25113; Δ*gshA*; Δ*dsbA*723::km	This study
Δ*dsbB* (JW5182-1)	BW25113; Δ*dsbB774*::km	(Baba et al., 2006)
Yeast strains		
YPH499	Δ*glr1*Δ*grx1*Δ*grx2*	(Zimmermann et al., 2021)

1003

1004   **Supplementary table 2. Plasmids used in this study**.

Plasmid	Relevant characteristics	Reference
Cloning/ template plasmids		
pPT	IPTG-inducible, pCC derivative, *torA*	This study
pCC	IPTG-inducible, TAC-MAT-Tag-2 derivative; p*tac,* Amp^R	(Degrossoli et al., 2018; Masuch et al., 2015)
pLK8 (pQE30-*roGFP-iL*)	roGFP-iL template, Amp^R	Addgene, USA, #83313 (Lohman and Remington, 2008)
p416TEF_roGFP2-AtPrxA-ΔCP	Yeast expression plasmid coding for AtPrxA-ΔCP, Amp^R	(Zimmermann et al., 2021)
E. coli expression plasmids		
pCC_*roGFP2*	pTAC-MAT-Tag-2 derivative; *roGFP2*, *ptac,* Amp^R	(Müller et al., 2017)
pPT	pTAC-MAT-Tag-2 derivative containing the N-terminal TorA TAT signal sequence	This study
pPT_*roGFP2*	pPT containing *roGFP2*	This study
pLK9 (pPT_*roGFP-iL*)	pPT containing *roGFP-iL*	This study
pOE1_*dsbA*ΔSP	pET11a-derivative, Strep-tag, TEV-site, *dsbA*ΔSP, Amp^R	Lab collection
Yeast expression plasmids		
pLK16 (p416TEF_roGFP2-*Ec*DsbAΔSP)	Yeast expression plasmid coding for *EcDsbA*ΔSP, Amp^R	This study
p415TEF-*OPT1*	Yeast expression plasmid coding for Opt1/Hgt1	(Zimmermann et al., 2021)
p416TEF_*roGFP2*	Yeast expression plasmid coding for roGFP2	(Zimmermann et al., 2021)
Removal of kanamycin cassette		
709-*Flpe*	*flpe*, λR promoter, heat-labile cI857 repressor Amp^R	Gene Bridges, Germany, #A106

1005

1006 **Supplementary table 3. Oligonucleotides used in this study**. Restriction and mutagenesis

1007 sites are underlined.

| Primer	Oligonucleotide sequence (5´→ 3´)
pPT plasmid for periplasmic targeting	
torA_NdeI-fwd	GGGGGCATATGAACAATAACGATCTCTTTCAG
torA_rev	GGAATACATATGCGCCGCTTGCGCCGCAGT
QC-Nde-fw	GGAGATATCGTATGAACAATAACGATCTCTTTCAG
QC-Nde-rv	CGTTATTGTTCATACGATATCTCCTGTGTGAAATTG
pPT_roGFP2 expression plasmid	
roGFP2_NdeI-fwd	AACCCCATATGGTGAGCAAGGGCGAGGA
roGFP-_EcoR -rev	GGGGGGAATTCTTACTTGTACAGCTCGTC
pLK9 (pPT_roGFPiL expression plasmid)	
roGFP-iL_XhoI-fwd	AAACTCGAGAAAAAGGAGAAGAACTTTTC
roGFP-iL_EcoRI-rev	AAAGAATTCTTATTTGTATAGTTCATCCATGC
pLK16 (p416TFE_roGFP2_*Ec*DsbAΔSP expression plasmid)	
DsbAΔSP_EcoRI-fwd	AAAGAATTCGCGCAGTATGAAGATG
DsbAΔSP_HindIII-fwd	TTTAAGCTTTTATTTTTTCTCGGACAGA
gshA removal	
gshA_fwd	AAATGTGTCTGTTAGCGGGATGGATGC
gshA_rev	AAAAGGCGCTTCCATCCGGGTATGATC
Δ*dsbA* insertion	
dsbA_fwd	AAATTTACGCGCCATGCGTTTGGTTT
dsbA_rev	AAATTACGGCTAACGCAACAATAACAC
KEIO primers (Baba et al., 2006)	
k1	CAGTCATAGCCGAATAGCCT
k2	GGTGCCCTGAATGAACTGC

1008
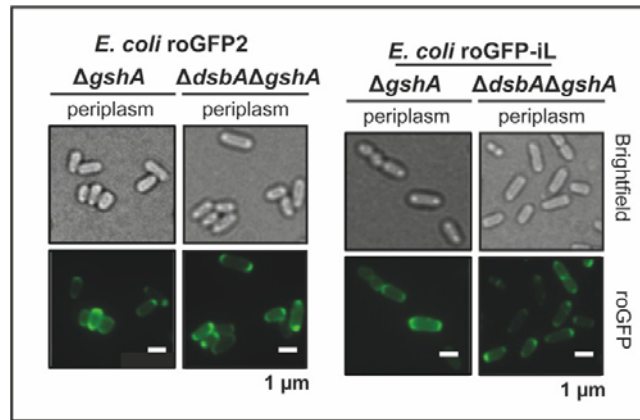
1009

1010 **Supplementary figure 2. roGFP probes localize in the periplasm of cells lacking GshA or DsbA and**
1011 **GshA.** Fluorescence microscopy of *E. coli* Δ*gshA* and Δ*dsbA*Δ*gshA* expressing roGFP2 (left) or roGFP-iL
1012 (right) confirming periplasmic localization of both roGFP probes.
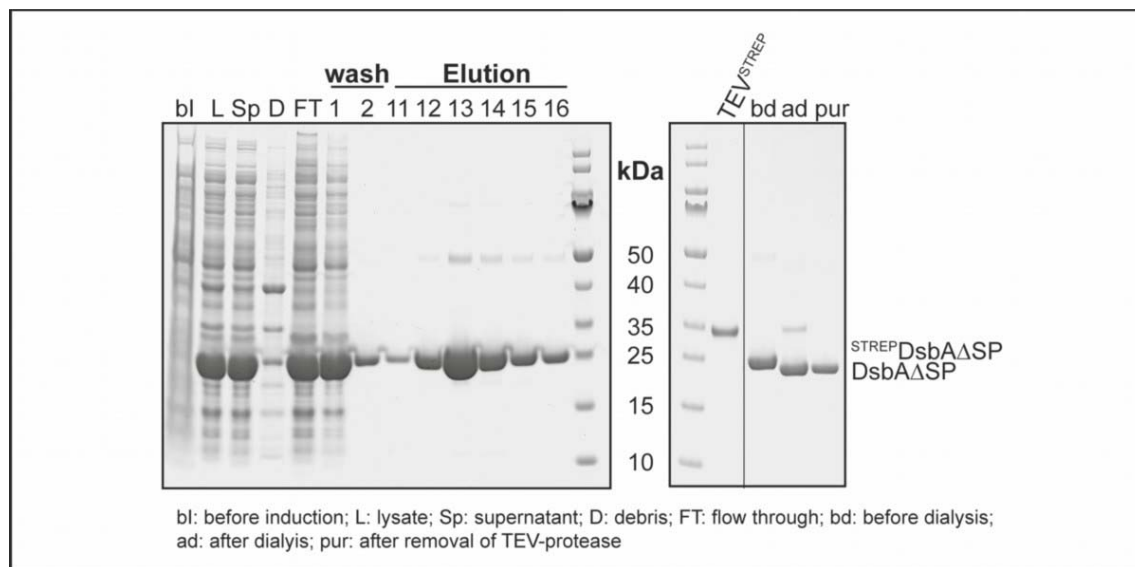
Supplementary figure 3. Purification of tag-free DsbAΔSP from *E. coli* BL21 cell lysate. SDS-PAGE of samples collected during the purification process. Cells harboring the plasmid for expression of STREPDsbAΔSP were grown to an OD_{600} of 0.6-0.8 (bI) before expression was induced for 20 h at 20 °C. Then cells were harvested and lysed (L) and the lysate was separated by centrifugation (30 min, 4 °C, 25.000 x g) into supernatant (Sp) and debris (D). The supernatant was loaded onto a Streptavidin column (StrepTrap™, GE Healthcare, Chicago, USA), washed with 5 CV buffer W (100 mM Tris-HCl, 150 mM NaCl, 1 mM EDTA, pH 8.0) and eluted with buffer E (100 mM Tris-HCl, 150 mM NaCl, 1 mM EDTA, 2.5 mM Desthiobiotin, pH 8.0) with the help of ÄKTApurifier (GE-Healthcare, Chicago, USA). Elution fractions were incubated over night at 4 °C during dialysis to buffer W with Strep-tagged TEV-protease (1:20 TEVSTREP: STREPDsbAΔSP) to get tag-free DsbA. The TEV-protease and uncleaved STREPDsbAΔSP were removed using a Streptavidin column resulting in pure DsbAΔSP (pur).

46
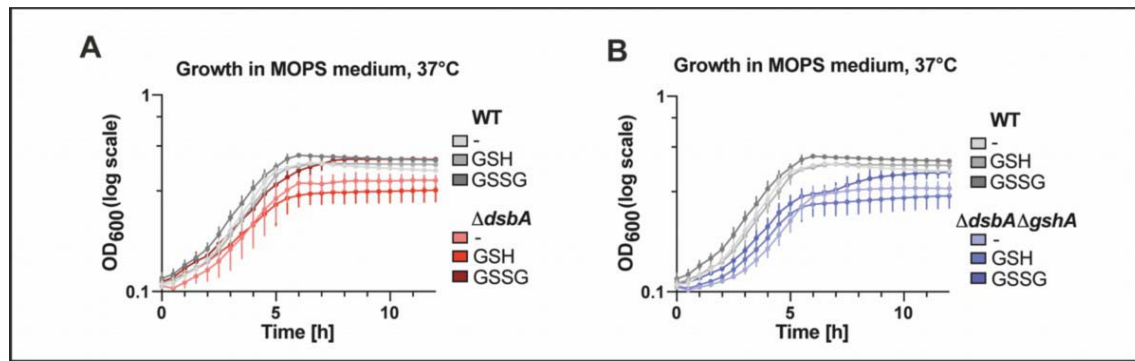
Supplementary figure 3. Supplementation of the growth medium with oxidized glutathione rescues growth of DsbA-deficient cells, while GSH has an inhibitory effect. *E. coli* WT (**A and B**), Δ*dsbA* (**A**) and Δ*gshA*Δ*dsbA* (**B**) were cultivated at 37 °C in MOPS minimal medium without or with supplementation of 5 mM GSH or GSSG. OD_{600} was recorded over time and for better visualization y-axis is shown in log scale. Presented values are the mean of three biological replicates recorded in duplicate assays and error bars represent the standard deviation.

1032
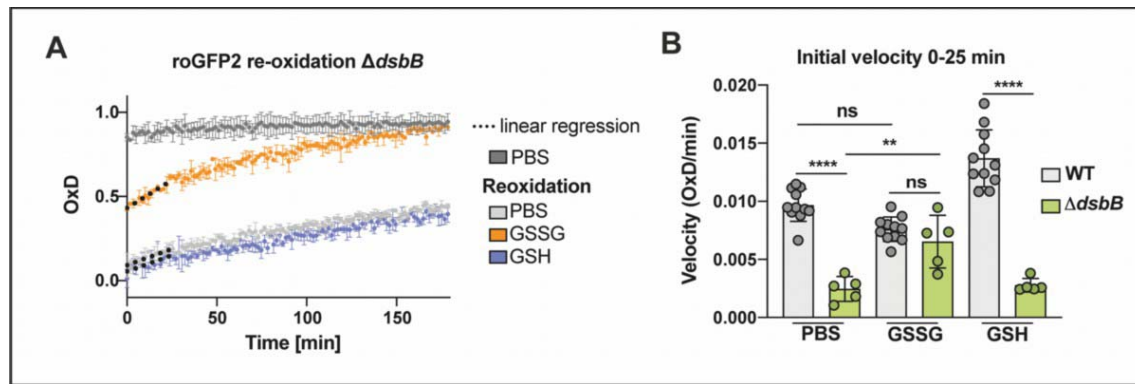
Supplementary figure 4. External addition of oxidized glutathione rescues the reoxidation of roGFP2 in the periplasm of cells lacking DsbB. (A) Reoxidation of periplasmic roGFP2 in *E. coli ΔdsbB*. Periplasmic reoxidation assay of roGFP2 in *E. coli ΔdsbB* was carried out as described in Fig. 3. One representative example out of at least five individual repeats is shown. Error bars represent standard deviation of technical triplicates. **(B)** The initial reoxidation velocity was calculated from linear regression in the first 25 min (dashed lines). Values (circles) are the mean of three technical replicates recorded in a minimum of five independent repeats. Error bars represent the standard deviation. Significance test was performed using one way ANOVA. **$p<0.01$, ****$p < 0.0001$.

1041   Baba, T., Ara, T., Hasegawa, M., Takai, Y., Okumura, Y., Baba, M., Datsenko, K.A., Tomita,
1042   M., Wanner, B.L., Mori, H., 2006. Construction of *Escherichia coli* K-12 in-frame,
1043   single-gene knockout mutants: the Keio collection. Molecular Systems Biology 2,
1044   2006.0008. https://doi.org/10.1038/msb4100050
1045   Blattner, F.R., Plunkett, G., Bloch, C.A., Perna, N.T., Burland, V., Riley, M., Collado-Vides,
1046   J., Glasner, J.D., Rode, C.K., Mayhew, G.F., Gregor, J., Davis, N.W., Kirkpatrick,
1047   H.A., Goeden, M.A., Rose, D.J., Mau, B., Shao, Y., 1997. The Complete Genome
1048   Sequence of *Escherichia coli* K-12. Science 277, 1453–1462.
1049   https://doi.org/10.1126/science.277.5331.1453
1050   Degrossoli, A., Müller, A., Xie, K., Schneider, J.F., Bader, V., Winklhofer, K.F., Meyer, A.J.,
1051   Leichert, L.I., 2018. Neutrophil-generated HOCl leads to non-specific thiol oxidation
1052   in phagocytized bacteria. eLife 7, e32288. https://doi.org/10.7554/eLife.32288
1053   Lohman, J.R., Remington, S.J., 2008. Development of a family of redox-sensitive green
1054   fluorescent protein indicators for use in relatively oxidizing subcellular environments.
1055   Biochemistry 47, 8678–8688. https://doi.org/10.1021/bi800498g
1056   Masuch, T., Kusnezowa, A., Nilewski, S., Bautista, J.T., Kourist, R., Leichert, L.I., 2015. A
1057   combined bioinformatics and functional metagenomics approach to discovering
1058   lipolytic biocatalysts. Frontiers in Microbiology 6.
1059   https://doi.org/10.3389/fmicb.2015.01110
1060   Müller, A., Schneider, J.F., Degrossoli, A., Lupilova, N., Dick, T.P., Leichert, L.I., 2017.
1061   Systematic *in vitro* assessment of responses of roGFP2-based probes to
1062   physiologically relevant oxidant species. Free Radical Biology and Medicine 106,
1063   329–338. https://doi.org/10.1016/j.freeradbiomed.2017.02.044
1064   Studier, F.W., Moffatt, B.A., 1986. Use of bacteriophage T7 RNA polymerase to direct
1065   selective high-level expression of cloned genes. Journal of Molecular Biology 189,
1066   113–130. https://doi.org/10.1016/0022-2836(86)90385-2
1067   Taylor, R.G., Walker, D.C., Mclnnes, R.R., 1993. *E. coli* host strains significantly affect the
1068   quality of small scale plasmid DNA preparations used for sequencing. Nucleic Acids
1069   Research 21, 1677–1678. https://doi.org/10.1093/nar/21.7.1677
1070   Zimmermann, J., Oestreicher, J., Geissel, F., Deponte, M., Morgan, B., 2021. An intracellular
1071   assay for activity screening and characterization of glutathione-dependent
1072   oxidoreductases. Free Radical Biology and Medicine 172, 340–349.
1073   https://doi.org/10.1016/j.freeradbiomed.2021.06.016